J. Fluid Mech. (2004), *vol.* 506, *pp.* 369–406. © 2004 Cambridge University Press
DOI: 10.1017/S0022112003007791 Printed in the United Kingdom

Scalar mixing in a forced non-reactive plane shear layer using a thermal analogue to species concentration

By JOHN M. WILTSE[1] AND ARI GLEZER[2]

[1]FLIR Systems Inc., Portland, OR 97224, USA

[2]Woodruff School of Mechanical Engineering, Georgia Institute of Technology, Atlanta, GA 30332, USA

(Received 5 September 2002 and in revised form 20 October 2003)

Scalar composition and mixing rates within a non-reactive plane shear layer between two uniform water streams were manipulated by surface actuators on the high-speed side of the flow partition. The scalar concentrations were assessed using a thermal analogue by maintaining a time-invariant temperature difference between the uniform streams upstream of the flow partition. The ratio of the smallest velocity and temperature scales was governed by the Prandtl number. Because in water $Pr \approx 7$ while the Schmidt number Sc for dyes and reactants is $O(1000)$, temperature concentrations in water are a better representation of scalar mixing in air in which $Sc = O(1)$. The effects of spanwise-uniform and -non-uniform actuation programs were investigated using arrays of discrete, individually controlled thin-film resistive heating elements that were surface-mounted on the flow partition. Spatial and temporal temperature distributions were measured phase-locked to the actuation waveform using a cross-stream array of closely spaced cold-wire sensors. These data were used to infer both the mixedness and the composition through the onset of mixing transition and quantify local and integral cross-stream mixing performance measures. Actuation programs that hastened mixing and significantly altered the composition of mixed fluid were identified.

1. Introduction

Mixing in plane shear layers is accomplished via entrainment of irrotational fluid from each stream by nominally two-dimensional spanwise (primary) vortices (e.g. Winant & Browand 1974), and three-dimensional motions that are induced by packets of (secondary) streamwise counter-rotating vortex pairs which form in the 'braids' region between adjacent spanwise vortices (e.g. Bernal & Roshko 1986) and directly affect the evolution of small-scale motions within their cores. The amount of mixed fluid that can be produced at any streamwise station is limited by the large-scale entrainment induced by the spanwise vortices and depends on the transverse (cross-stream) extent of the shear layer and on the mixed fluid fraction (i.e. the ratio of mixed fluid to total (mixed and unmixed) fluid within the layer). The three-dimensional motions that are induced by the streamwise vortices and are necessary for the initiation of small-scale mixing are induced by a hierarchy of vortical structures of decreasing scales that continuously break down and strain the entrained fluid until diffusion of kinetic energy ultimately takes over at the smallest spatial scales followed by scalar diffusive processes (e.g. Dimotakis 1989). Given that both the primary and secondary

vortical structures result from two- and three-dimensional instabilities of the base flow, the manipulation of the instability modes that lead to their formation is a key to the control of mixing between the streams.

Mixing in both non-reactive and reactive single-phase plane shear layers between gas or liquid streams that are characterized respectively by high and low molecular diffusivity (as may be measured by the Schmidt number, Sc) has been the subject of a number of experimental investigations. Key studies in gaseous layers (i.e. $Sc = O(1)$), include the works of Konrad (1976), Batt (1977), Masutani & Bowman (1986) and Pickett & Ghandhi (2001, 2002), and in liquid layers (i.e. $Sc = O(1000)$) include the works of Breidenthal (1981), Koochesfahani & Dimotakis (1986), and Karasso & Mungal (1996). These investigations typically focused on three main areas: the characterization of the mixing transition (specifically the flow parameters that govern its onset, and the resulting changes in observable features in the flow), the variation of the composition of the mixed fluid across the shear layer, and finally, the role of molecular diffusivity (i.e. the Schmidt number) in turbulent mixing (specifically the differences in mixing between gaseous and liquid shear layers).

In early works, the mixing transition was characterized almost exclusively by the Reynolds number $Re_\delta = \Delta U \delta / \nu$. For example, using shadowgraph imaging in the cross-stream (x–y) and planform (x–z) planes of a gaseous plane mixing layer between helium and nitrogen, Konrad (1976) showed that above a critical Reynolds number, hairpin (streamwise) vortices develop in the 'braids' region between the primary vortices. The shadowgraph images suggested that the streamwise vortices are continuously stretched by and rolled into the primary vortices thereby leading to three-dimensional small-scale motions within the primary vortices and to substantial mixing enhancement. Concentration measurements (using a high-resolution concentration probe) showed that the composition of the mixed fluid does not vary significantly in the cross-stream direction as evidenced by the fact that the peaks in concentration probability density function (p.d.f.) are approximately the same at all cross-stream elevations. (This type of p.d.f. has since been denoted by Mungal & Dimotakis 1984 a 'nonmarching' p.d.f.). In another investigation in a chemically reacting gaseous mixing layer between N_2O_4 and N_2, Batt (1977) used a fibre-optic probe to measure concentrations of NO_2. In contrast to the findings of Konrad, the concentration p.d.f.s measured by Batt had 'marching' peaks in the cross-stream direction that tracked the time-averaged concentration. Although based on these findings Batt concluded that the spanwise vortices play only a limited role in the mixing process, later investigations (e.g. Mungal & Dimotakis 1984) attributed this result to the limited resolution of his measurements.

Measurements of the chemical composition within a non-reactive and reactive liquid shear layer using laser-induced fluorescence (Koochesfahani & Dimotakis 1986) showed that the concentration levels corresponding to the peaks of the p.d.f.s are virtually invariant with cross stream elevation (i.e., 'nonmarching' p.d.f.s). The authors noted that the expected values of the mixed fluid concentration become closer to the concentration of the low-speed stream with downstream distance, and suggested that this is the result of the entrainment of excess high-speed fluid during the initial rollup of the spanwise vortices which is then gradually depleted with downstream distance. Dimotakis (1989, 2000) concluded that mixing transition in an unforced two-stream shear layer is a function primarily of the Reynolds number, and occurs at $Re_m = \Delta U \delta / \nu \approx 10^4$, where $\Delta U = U_1 - U_2$ and $\delta = \delta(x)$ is the local cross-stream extent of the shear layer. Although they did not measure scalar mixing directly, Huang & Ho (1990) studied mixing layer growth and the onset of

small-scale transition by measuring the velocity field. They found that the merging of the spanwise vortices as well as small-scale transition (as measured by the roll-off exponent of the velocity power spectra) are influenced by the 'pairing parameter' $X = Rx/\lambda_0$ (the first and second mergings occur at $X = 4$ and 8, respectively), that has since been extensively used in studies of scalar mixing (e.g. Karasso & Mungal 1996). In this definition, R is the ratio of deformation to advection velocities, $(U_1 - U_2)/U_{ave}$, and λ_0 is the initial instability wavelength, which was calculated from the vortex passage frequency $\lambda_0 = U_{ave}/f_0$. The data of Huang & Ho (1990) show that small scales in the flow (necessary for mixing) develop within the range $4 \leqslant Rx/\lambda_0 \leqslant 8$.

In an investigation of scalar mixing in both reactive and non-reactive liquid plane shear layers, Karasso & Mungal (1996) validated the earlier observations of Koochesfahani & Dimotakis just past the mixing transition. Karasso & Mungal showed that the evolution of the scalar field, including mixing transition, scales with the pairing parameter Rx/λ_0. They also showed that these features of the flow are not uniquely determined by the Reynolds number because it does not account for the inflow conditions (namely, initial boundary layer thickness). Using resolution-independent chemical-reaction data, they found that the true p.d.f. evolves from non-marching to 'tilted' (i.e. having a small cross-stream variation in mixed fluid concentration) downstream of the mixing transition at $Rx/\lambda_0 > 22$ (just past the third merging of the spanwise vortices).

In mixing experiments in a high-Schmidt-number chemically reacting liquid shear layer between phenolphthalein and sodium hydroxide, Breidenthal (1981) used a pH indicator to form a visible product to quantify the mixing. Similar to the earlier results of Konrad, Breidenthal found that mixing transition occurs when streamwise vortices appear in planform views of the shear layer. However, while downstream of the mixing transition the Schmidt number appears to have a relatively weak effect on the mixing (the product thickness in the liquid layer is only about half the thickness in gas even though the difference in the Schmidt number is almost three orders of magnitude), its importance is far more significant upstream of mixing transition. Within this domain, the measurements in the liquid shear layer show virtually no appreciable mixing and product formation while the measurements in air (e.g. Konrad 1976) exhibit significant mixing.

Later experiments in a chemically reacting gaseous plane shear layer (Masutani & Bowman 1986) also demonstrated significant mixing upstream of mixing transition that was similar to the findings of Konrad (1976) and in contrast to mixing measurements in liquids (Breidenthal 1981; Koochesfahani & Dimotakis 1986). Masutani & Bowman attributed the enhanced mixing in low-Schmidt-number flows in the absence of significant three-dimensional motions to higher molecular diffusivity. They suggested that, consistent with the model of Broadwell & Breidenthal (1982), mixing in a gas layer takes place both in thin diffusion zones wrapped around the primary vortices ('flame sheet' mixing) and in homogeneously mixed zones at the centres of the primary vortices. While the 'flame sheet' mixing occurs at all concentrations, the homogeneous mixing occurs preferentially at a concentration that is determined by the entrainment ratio. Pickett & Ghandhi (2001, 2002) investigated the effects of inlet conditions on mixing in a gas shear layer and concluded that mixing transition is essentially complete at $Re_\delta \approx 5000$, where the mixed fluid fraction reaches an asymptotic value of approximately 0.5. They found significant mixed fluid even far upstream from that location which they attributed to the 'flame sheet' mixing of Broadwell & Breidenthal (1982).

The investigations in unforced plane shear layers are important because they provide a solid background for understanding the mixing mechanisms and therefore help put the present work in context. A novel feature of the present experiments is the use of temperature (rather than dyes or reactants) as a passive scalar, so the ratio of the smallest velocity scales to the smallest temperature scales is governed by the Prandtl number instead of the Schmidt number. Since in water, $Sc = O(1000)$ and $Pr \approx 7$ (compared to $O(1)$ for both in air), mixing of temperature in water is a closer analogue to mixing in air, in which earlier investigation reported significant 'flame sheet' mixing. The present measurements were obtained for $1.2 \leqslant Rx/\lambda_0 \leqslant 5.4$, with a corresponding Re_δ in the range of $0.36 \times 10^{-4} \leqslant Re_\delta \leqslant 1.73 \times 10^{-4}$. While the mixing field is clearly not fully developed (e.g. Karasso & Mungal 1996), this streamwise domain in the present flow includes the middle stage of mixing transition, as is evidenced by the presence of substantial levels of mixed fluid even in the absence of forcing (i.e. the baseline flow). The mixing transition is thus partially complete.

While the receptivity of the base flow to time-harmonic excitation has been used to substantially modify its global features (e.g. Oster & Wygnanski 1982; Nygaard & Glezer 1991), only a few investigations have directly considered or measured the effects of the actuation on mixing. Roberts & Roshko (1985) used relatively high-level time-harmonic actuation to manipulate the mixing within a chemically reacting shear layer. These authors reported that while forcing at subharmonics of the 'natural' (i.e. most unstable) frequency of the base flow typically results in increased mixing downstream of mixing transition, forcing at the 'natural' frequency arrests the growth of the spanwise vortices and consequently inhibits the mixing within a 'phase-locked' domain (where the forcing is most effective). Koochesfahani & MacKinnon (1991) and Katch & Koochesfahani (1993) found that the enhancement of mixing as a result of forcing below the 'natural frequency' is the result of increased entrainment, and that mixing is enhanced preferentially at concentrations close to that of the high-speed stream.

The primary focus of the present work is to investigate the changes in mixing within the domain of mixing transition in the flow as a result of excitation of the fundamental instabilities of the base flow. Mixing is enhanced by altering both primary flow mechanisms that affect mixing, namely entrainment and small-scale motions. These flow mechanisms are affected by the spanwise and streamwise vortical structures within the shear layer (i.e. entrainment and small-scale motions, respectively) and therefore can be regulated by independent manipulation of the two- and three-dimensional flow instabilities that lead to the formation of these vortices. The phase reference that is provided by time-harmonic actuation is used for investigation of the phase-averaged structure of the flow with specific emphasis on the flow domains where mixing occurs. The experimental apparatus and techniques are described in § 2. Instantaneous scalar concentrations (i.e. temperature) and the time-averaged mixing performance measures are presented in § 3 and § 4 for the unforced and the forced flow, respectively. Concentration measurements that are acquired phase-locked to the actuation waveform are presented in § 5. Finally, concluding remarks are presented in § 6.

2. Experimental apparatus and procedure

2.1. *The water shear layer facility and instrumentation*

The experiments were conducted in a closed-return water facility shown schematically in figure 1(*a*). A detailed view of the flow partition (including the coordinate system) is shown in figure 1(*b*). The two-stream shear layer facility and some of its auxiliary

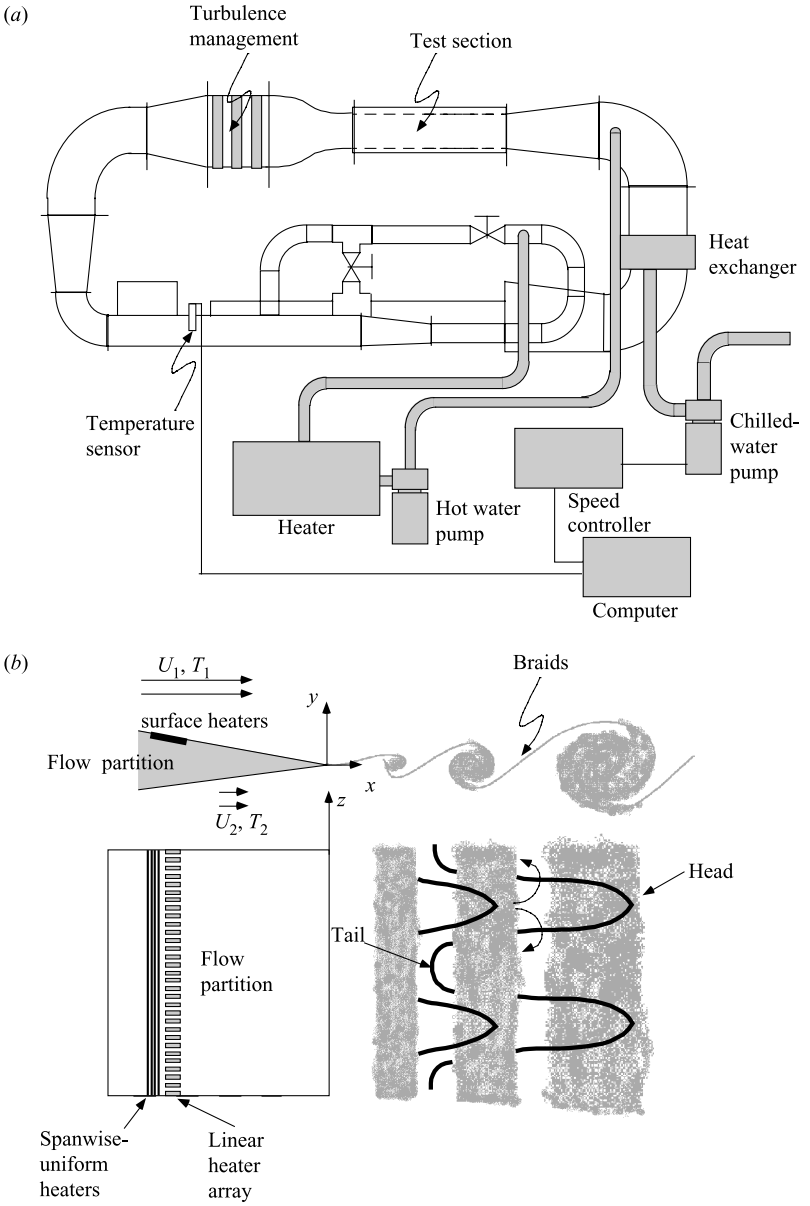

FIGURE 1. (*a*) The two-stream mixing layer facility, and (*b*) the flow partition, surface heaters, coordinate system, and flow topology.

equipment are described in detail in Nygaard & Glezer (1991) and Wiltse (1993). The spanwise width of the test section was approximately 21.3 cm. In order to minimize sidewall contamination, the present data were acquired within a spanwise domain that was 6 cm wide and symmetric about the centre span (i.e. at a distance of at least 7 cm from either wall). In the present study, the velocities of the high-speed and low-speed free streams were $U_1 = 36$ and $U_2 = 12\,\mathrm{cm\,s^{-1}}$, respectively. The boundary layers on either side of the flow partition were laminar, with estimated (by the method of Thwaites) momentum thicknesses of 0.06 cm and 0.10 cm on the high-speed and

low-speed sides, respectively. The corresponding Reynolds numbers were $Re_\theta = 248$ and 133, respectively.

To provide a constant temperature difference between the two free streams (3 °C, in the present experiments), the water channel was equipped with a circulation heater upstream of the return circuit, and a chilled-water heat exchanger downstream of the diffuser. Water from the diffuser was pumped at $1.3\,\mathrm{l\,s^{-1}}$ through the 63 kW circulation heater where the temperature was raised by approximately 10 °C. The heated water was then injected through multiple jets into the low-speed flow, well upstream of the turbulence management devices. The chilled-water side of the heat exchanger was operated at nominally $3.8\,\mathrm{l\,s^{-1}}$ and 8 °C, while the flow rate of circulated mixed shear layer fluid was regulated by the laboratory computer so that the temperatures of the free streams were maintained within ± 0.03 °C of their set values. In the present experiments, the temperatures of the high- and low-speed streams were $T_1 = 25$ °C and $T_2 = 28$ °C, respectively.

As noted in § 1, the receptivity of the nominally two-dimensional shear layer to controlled two- and three-dimensional perturbations was exploited for the manipulation of the evolution of vortical structures within the base flow and consequently the mixing between the two streams. Spanwise-uniform and -non-uniform vorticity perturbations were introduced into the high-speed flow partition boundary layer by exploiting the dependence of viscosity on temperature (Liepmann, Brown & Nosenchuck 1982) using an array of surface heating films. As illustrated in figure 1(*b*), the array was composed of four spanwise-uniform elements upstream of a 32-element spanwise row and each heating element was driven independently by a dedicated DC power amplifier. The driving signal to the heating elements was provided by a custom-built 36-channel, high-speed, dual-mode D/A converter where channels are individually addressable either as a programmable arbitrary (time-periodic) waveform generator or as an updateable source for real-time control (Wiltse 1993). The average wall temperature rise at the heater was approximately 22 °C, which diffused into the high-speed boundary layer. The average temperature rise at the end of the flow partition was only 0.1 °C.

2.2. *Temperature measurements*

The temperature distribution within the shear layer was measured using a rake of 31 cold wire sensors spaced 2 mm apart, spanning a total cross-stream (y) distance of 6 cm. Each sensor was composed of a 10 μm diameter, 1.6 mm long, platinum–iridium wire. The fluid temperature was measured using a 31-channel cold-wire thermometer (CWT) that was designed and built for the purposes of the present experiments. Each CWT channel has an r.m.s. noise fluctuation of approximately 0.025 °C and an overall temperature resolution (including switching noise) of 0.03 °C. The CWT channels were scanned (triggered by the laboratory computer) using a high-speed analogue switch having a maximum rate of 100 kHz. The cold-wire rake was mounted on a computer-controlled traversing mechanism and calibrated to a linear fit between the response in each free stream. The calculated frequency response (Perry 1982, p. 48) was 3.2 kHz.

The present temperature measurement technique has inherent spatial and temporal resolution limitations. If the cold-wire-sensor is significantly longer than the smallest temperature scale in the flow (i.e. the Batchelor scale η_B) spanwise temperature variations are averaged along its length and falsely interpreted as mixed fluid. The sensor also low-pass filters the temperature signal below the frequency U_c/l_w (where the convection velocity $U_c = (U_1 + U_2)/2$ and l_w is the sensor length). The

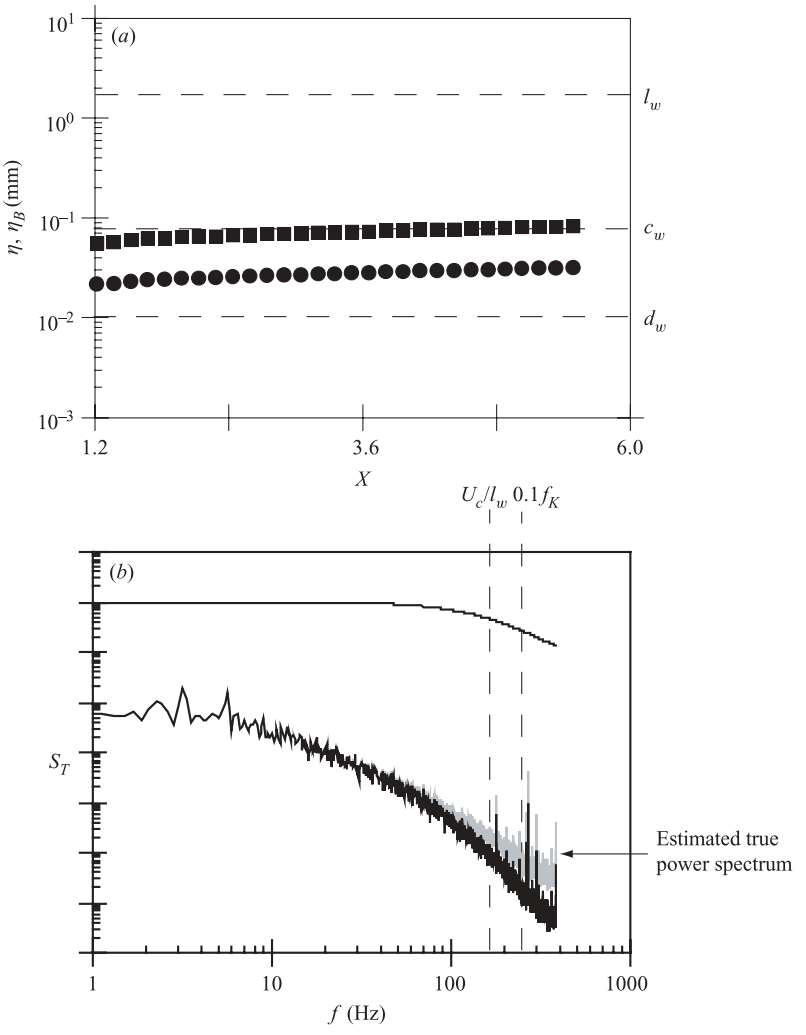

FIGURE 2. (*a*) Estimated Kolmogorov scale η (■) and Batchelor scale η_B (●) for the unforced flow. Shown for reference is the cold-wire diameter ($d_w = 10\,\mu$m) and length ($l_w = 1.6$ mm) as well as the convection wavelength (c_w). (*b*) Spectrum of temperature variance $S_T(f)$ along the centreline at $Rx/\lambda_0 = 5.40$ for the unforced flow. The top curve is a single-pole low-pass filter at U_c/l_w, and the estimated true power spectrum is shown in grey. Also shown for reference are the two frequencies $0.1f_K$ and U_c/l_w.

Kolmogorov and Batchelor scales are estimated (for homogeneous isotropic turbulent flow) as $\eta = 2\delta/Re_\delta^{3/4}$ and $\eta_B = \eta/Pr^{1/2}$, respectively, where δ is the shear layer width. Figure 2(*a*) shows the estimated Kolmogorov and Batchelor scales as a function of streamwise position for the unforced flow. Also shown for reference are the sensor length ($l_w = 1.6$ mm) and diameter ($d_w = 10\,\mu$m) and a convective wavelength c_w based on the frequency response of the cold-wire thermometer (3.2 kHz) and the convection velocity U_c.

Clearly, the finite wire length is the limiting factor for resolution and frequency response. The degree to which this is the case can be assessed by considering two types of data. A wire of finite length should low-pass filter the temperature signal at a

frequency corresponding to U_c/l_w. Figure 2(*b*) shows a plot of the power spectrum of the temperature variance at $Rx/\lambda = 5.40$ and $Y = Z = 0$ for the unforced flow. Noted for reference are U_c/l_w and $0.1 f_K$, where f_K is the 'Kolmogorov frequency' $f_K \equiv U_c/\eta$. The power spectrum of an unbiased temperature signal is expected to roll off at frequencies higher than about $0.1 f_K$. The figure shows the estimated 'true' power spectrum that would be measured if the cold wire did not act as a low-pass filter at U_c/l_w. Although the finite wire length clearly had some effect on the power spectrum between U_c/l_w and $0.1 f_K$, this effect is minor and appears to be secondary to the natural cut-off within the flow. Furthermore, since the magnitude of the spectral component at U_c/l_w was about three orders of magnitude smaller than that at the low-frequency peaks, it is likely that the incidence of these scales was not common, and that any overestimation of the mixed fluid due to averaging of these scales was quite small.

2.3. *Mixing performance measures*

Cross-stream temperature measurements were used to quantify mixing via three measures: the instantaneous performance measure, p.m., the integral performance measure, PM, and the probability density function of temperature, p.d.f. Temperature was non-dimensionalized as $\theta = (T - T_1)/(T_2 - T_1)$, such that $\theta_1 = 0$ and $\theta_2 = 1$ in the high- and low-speed streams, respectively. The instantaneous performance measure of mixing is defined as

$$\text{p.m.}(\boldsymbol{X}, t) = (1 - \theta)\theta,$$

where $0 \leqslant \theta(\boldsymbol{X}, t) \leqslant 1$ and the flow coordinates $\boldsymbol{x} = (x, y, z)$ are normalized by the pairing parameter such that $\boldsymbol{X} = R\boldsymbol{x}/\lambda_0$ (where λ_0 is the most unstable wavelength of the unforced base flow, and $R = \Delta U/U_{ave} = (U_1 - U_2)/0.5^*(U_1 + U_2) = 1$). In the present experiments $\lambda_0/R = 4.24$ cm. The quadratic performance measure is non-negative within the mixing region, vanishes when θ is either 0 or 1, and has a maximum value of 0.25 when $\theta = 0.5$ (i.e. the average temperature of the free streams). Analogous to the momentum thickness in velocity field measurements, the dimensionless integral performance measure PM represents the overall cross-stream amount of mixed fluid at a given spanwise and streamwise position:

$$\text{PM}(X, Z, t) = \int_{-\infty}^{\infty} \text{p.m.}(X, Y, Z, t)\, \mathrm{d}Y.$$

The likelihood that the temperature of a fluid element at a given position $\boldsymbol{X}$ within the flow is within the range $\theta_A \leqslant \theta < \theta_B$ is determined using the probability density function p.d.f.$(\theta, \boldsymbol{X})$:

$$\text{p.d.f.}(\theta)|_{X,Y,Z} = \operatorname*{Lim}_{(\theta_B - \theta_A) \to 0} \left[\frac{P(\theta_A \leqslant \theta < \theta_B)}{\theta_B - \theta_A} \right].$$

An important advantage of passive scalar techniques is that they allow direct determination of the complete composition of the mixed fluid in the form of the p.d.f. and quantities derived from it.

As noted in § 1, Mungal & Dimotakis (1984) attribute the presence of 'marching' p.d.f.s (where the peak temperature changes with cross-stream position) to inadequate resolution. The fraction of time that the sensor encounters fluid from a given stream is greater the closer it is to that stream. If the sensor has inadequate resolution (i.e. the measurement volume includes both unmixed and mixed fluid), then because the ratio of unmixed fluids is weighted according to the mean concentration profile, the peak in the p.d.f. tends to 'march' (vary) in conjunction with the mean concentration

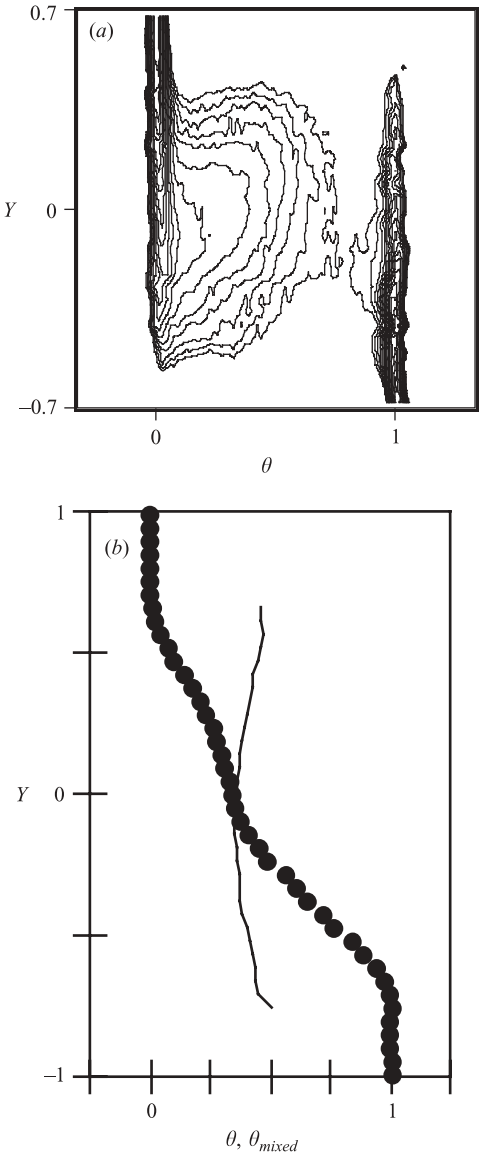

FIGURE 3. (*a*) Probability density function of temperature p.d.f.(θ, Y) for the unforced flow at $Rx/\lambda_0 = 5.40$, and (*b*) time-averaged profiles of temperature $\theta(Y)$ (●) and mixed fluid temperature $\theta_{mixed}(Y)$ (——) for the unforced flow at $Rx/\lambda_0 = 5.40$. The contours of $\log_{10}$(p.d.f.(θ, Y)) begin at a minimum level of -0.523 with a contour increment of 0.1.

profile. A sample p.d.f. at $Rx/\lambda_0 = 5.40$ for the present base (unforced) flow (figure 3*a*) shows no evidence of a marching peak. The mean mixed fluid temperature, θ_{mixed}, and the average fluid temperature, θ, are derived from the p.d.f. as follows:

$$\theta_{mixed}(Y) = \frac{\displaystyle\int_{\varepsilon}^{1-\varepsilon} \theta \,\text{p.d.f.}(\theta, Y)\,\mathrm{d}\theta}{\displaystyle\int_{\varepsilon}^{1-\varepsilon} \text{p.d.f.}(\theta, Y)\,\mathrm{d}\theta},$$

for

$$\int_{\varepsilon}^{1-\varepsilon} \text{p.d.f.}(\theta, Y)\,\mathrm{d}\theta \geqslant 0.1$$

and

$$\theta(Y) = \int_{0}^{1} \theta\ \text{p.d.f.}(\theta, Y)\,\mathrm{d}\theta.$$

$\theta(Y)$ and $\theta_{mixed}(Y)$ are shown in figure 3(*b*). If the p.d.f. were marching, θ_{mixed} would follow θ and this is clearly not the case. It is noteworthy that, in contrast to species concentration measurements, temperature measurements have reduced requirements on resolution. The smallest temperature scales are only slightly smaller than the smallest velocity scales ($Pr^{1/2} \approx 2.6$), whereas the smallest species diffusion scales are an order of magnitude smaller.

Finally, it is noted that similar to other passive scalar techniques, the present measurements yielded an upper bound on the amount of mixed fluid within the shear layer. The present investigation was primarily concerned with the use of actuation at the flow boundary to enhance mixing, and therefore with the change in mixing in the presence or absence of actuation. Indeed, much of the present data are shown in terms of the relative change compared to the baseline flow.

3. Mixing in the unforced shear layer

The mixing in the unforced shear layer is characterized using composites of temperature data measured at the streamwise stations $Rx/\lambda_0 = 2.4$, 3.6, and 4.8 as shown in figure 4(*a–c*), respectively. Each composite includes (from left to right) a plot of the time-averaged cross-stream temperature distribution $\theta(Y)$, a greyscale raster image of the instantaneous cross-stream temperature distribution $\theta(Y, t)$ over a period of 0.67 s ($3.8T_0$ where T_0 is the characteristic period of the unforced flow), and a contour plot of p.d.f.(θ, Y). The contour plot of the probability density function is shown using a logarithmic scale to better elucidate the lower mixing levels (which, over a large region, contribute extensively to the mixing) by comparison to the two lobes (at $\theta_1 = 0$ and $\theta_2 = 1$) in the free streams. Cross-stream distributions of the instantaneous temperature at four instances during the temperature time record are shown on the right-hand side of the figure.

At $Rx/\lambda_0 = 2.40$ (figure 4*a*), the distribution of p.d.f.(θ, Y) shows that there was virtually no mixed fluid at this location. Of particular note is the cross-stream distribution of the mean temperature $\theta(Y)$, which has three inflection points separating two distinct bends: one towards θ_2 near the high-speed side and the other towards θ_1 near the low-speed side. Given the absence of mixing, these bends are apparently the result of the protrusion of unmixed layers of low- and high-speed fluid towards the opposite side of the shear layers as shown in the greyscale images of the instantaneous temperature distribution. The proximity of the centre inflection point to the high-speed side of the shear layer ($Y \approx 0.10$) indicates local excess of high-speed fluid. In the absence of mixing, the mean cross-stream temperature distribution depends on the time fraction that each of the sensors measures either θ_1 or θ_2. The presence of unmixed alternate layers of fluid from each stream within the cores of the primary vortices was evident in cross-stream distributions of instantaneous temperature at times t_1, t_2, and t_3. As the primary vortices were advected downstream, these layers were strained, became thinner, and their surface areas increased. At $Rx/\lambda_0 = 3.60$, p.d.f.(θ, Y) shows some increase in mixing near the high-speed side where the penetrating layers of

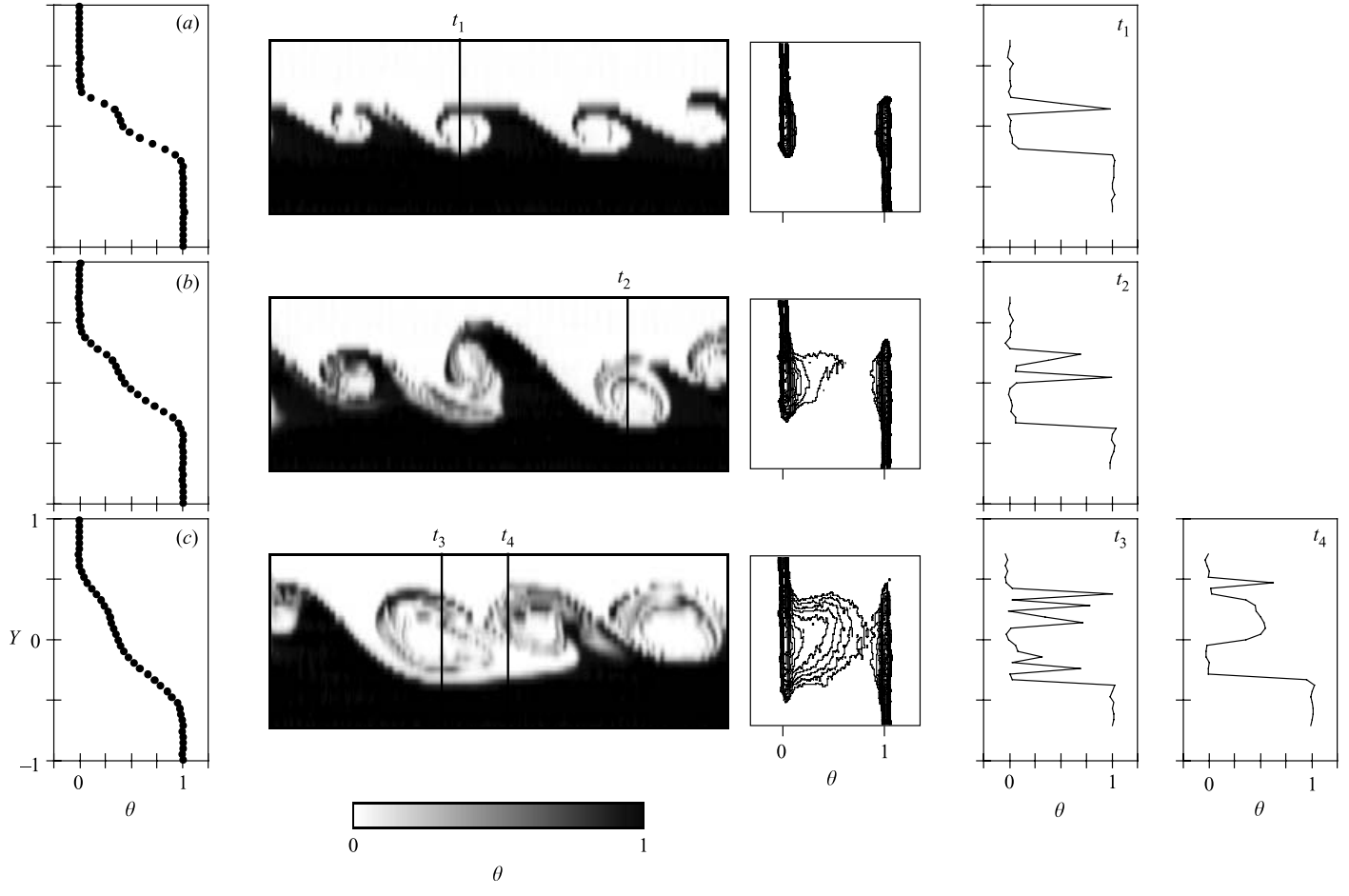

FIGURE 4. $\theta(Y)$, $\theta(Y, t)$, and p.d.f.(θ, Y) for the unforced flow at (*a*) $Rx/\lambda_0 = 2.40$, (*b*) 3.60, and (*c*) 4.80. Instantaneous temperature profiles $\theta(Y; t_i)$ are shown at times t_1, t_2, t_3, and t_4. The contours of $\log_{10}$(p.d.f.(θ, Y)) begin at a minimum level of -0.523 with a contour increment of 0.1.

low-speed fluid were relatively thin. Finally, at $Rx/\lambda_0 = 4.80$ the shear layer appears to be undergoing mixing transition; however, the p.d.f.(θ, Y) still does not have a distinct local maximum between the two streams. As is evident from the greyscale maps, mixing occurred primarily around the high- and low-speed edges of the spanwise vortices, suggesting the presence of naturally occurring streamwise vortices that are wrapped around the cores of the primary vortices (e.g. Nygaard & Glezer 1991) and are stretched along the 'braids' region. While the instantaneous temperature distributions at t_3 show some evidence of several layers of unmixed fluid within the primary vortices, at t_4 (near the downstream edge of the primary vortex) there was a large patch of mixed fluid.

Koochesfahani & Dimotakis (1986) studied mixing transition in a layer with $Sc \approx 600$. Their concentration p.d.f. for post-mixing transition ($Re = 23\,000$) showed a strong peak at a preferred concentration which is nominally invariant across the layer. Even though the present data were obtained at a somewhat lower Reynolds number ($Re = 14\,900$), the differences between the corresponding p.d.f.s are noteworthy. It appears that owing to the higher value of the effective diffusion coefficient, the mixing in the present experiments was affected by 'flame sheet' mixing, as is evidenced by the broader range of mixed temperatures compared to the experiments of Koochesfahani & Dimotakis (more 'homogeneous').

4. Mixing in the forced shear layer

In the present experiments, the shear layer was excited using spanwise-uniform (SU) and spanwise-periodic (SP) actuation waveforms. Spanwise-uniform actuation was achieved using the entire array of heating elements while the spanwise-periodic actuation waveform had a spanwise wavelength of 2.66 cm ($Z = 0.55$ in non-dimensional units) and a duty cycle of 75% (i.e. every fourth spanwise heater in figure 1(*b*) was driven at 4% of the power of its adjacent elements).

Similar to figure 4, figures 5–8 are composites of $\theta(Y)$, $\theta(Y, t)$ and p.d.f.(θ, Y) for the forced flow. In figure 5(*a–c*) ($Rx/\lambda_0 = 2.40$, 3.60, and 4.80, respectively) the actuation waveform was spanwise uniform and the forcing frequency was $f = 6$ Hz, which was quite close to the nominal 'natural' frequency of the flow (5.66 Hz). The present measurements show that the flow was phase-locked to the actuation waveform and that the streamwise growth rate and the degree of interaction between adjacent primary vortices was substantially reduced within the domain of measurement (cf. Oster & Wygnanski 1982). As a result of the actuation, the rollup of the primary vortices began farther upstream than in the unforced flow as is demontrated by a comparison of the degree of advection and penetration of fluid from both streams towards the centre of the vortices in corresponding distributions of $\theta(Y, t)$ at $Rx/\lambda_0 = 2.40$ in figures 4 and 5. This is also demonstrated by the instantaneous cross–stream temperature distributions $\theta(Y; t_5)$ ($Rx/\lambda_0 = 2.40$) and $\theta(Y; t_6)$ ($Rx/\lambda_0 = 3.60$) that reveal an increased number of thin temperature sheets compared to the corresponding distributions in the unforced flow (figures 4*a* and 4*b*). The time-averaged cross-stream temperature distribution at $Rx/\lambda_0 = 2.40$ shows that $\theta(Y)$ above the inflection point in the forced flow was higher than in the unforced flow (figure 4) indicating that more low-speed fluid was entrained towards the high-speed side by the accelerated evolution of the primary vortices. As a result of the organized rollup in the forced flow, there was an increase in the concentration of mixed fluid at warmer temperatures at $Rx/\lambda_0 = 3.60$ (near $Y = 0.10$) compared to the unforced flow (cf. p.d.f.(θ, Y) in figure 4*b*).

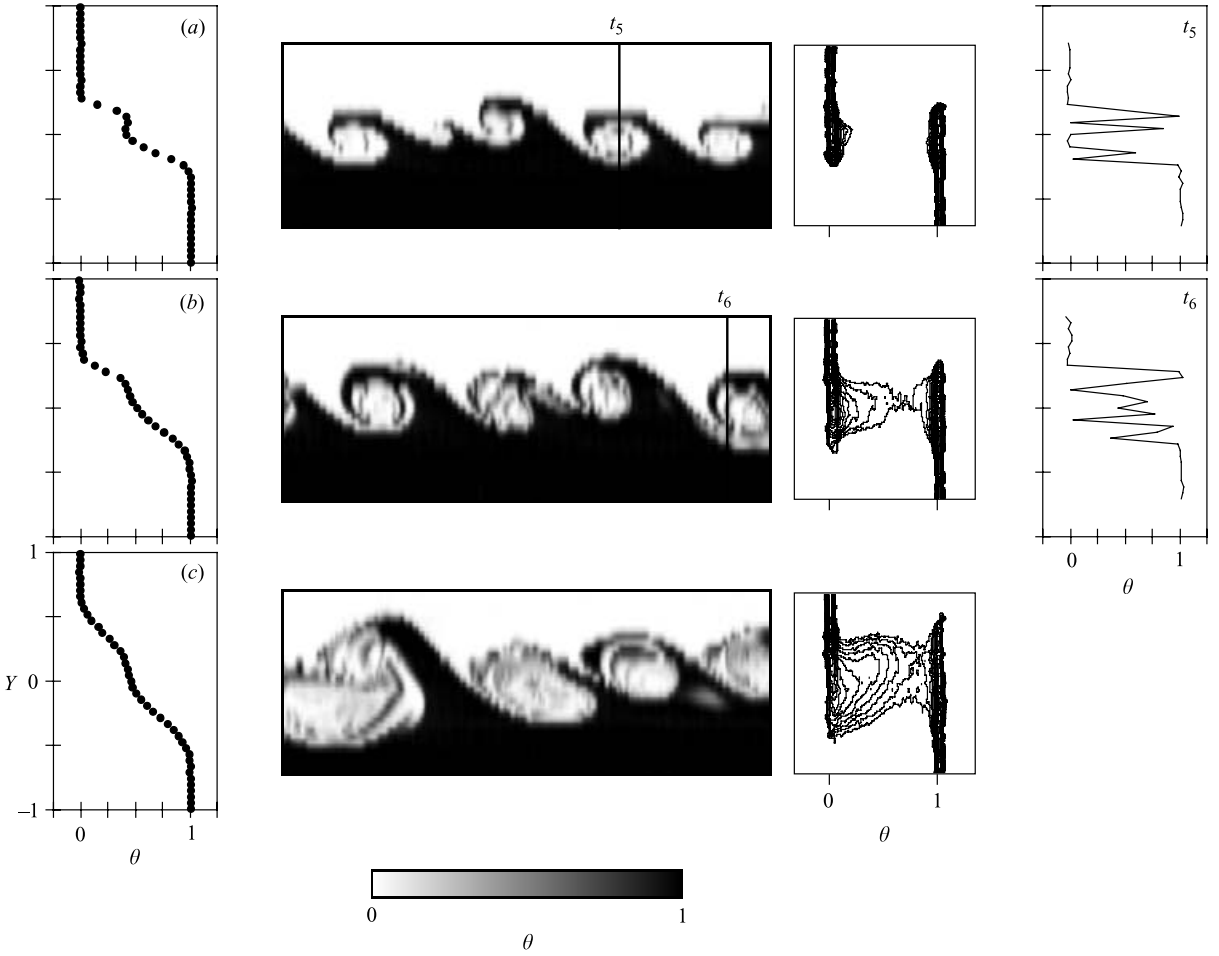

FIGURE 5. $\theta(Y)$, $\theta(Y,t)$, and p.d.f.(θ, Y) for SU forcing at $f = 6\,\mathrm{Hz}$ at (*a*) $Rx/\lambda_0 = 2.40$, (*b*) 3.60, and (*c*) 4.80. Instantaneous temperature profiles $\theta(Y;t_i)$ are shown at times t_5 and t_6. The contours of $\log_{10}$(p.d.f.(θ, Y)) begin at a minimum level of -0.523 with a contour increment of 0.1.

Despite the increase in mixing, it is noteworthy that the cross-stream width of the flow domain containing mixed fluid was somewhat narrower than in the unforced flow. This is consistent with the observation that forcing the shear layer near its natural frequency inhibits pairing and cross-stream spreading of the layer. At $Rx/\lambda_0 = 4.80$ (figure 5*c*) the cross-stream peak of p.d.f.(θ, Y) is somewhat narrower than that of the unforced flow (particularly near $\theta = 0.5$) but has a higher level of mixing, particularly near $\theta = 1$. This finding is in contrast to the observations of Koochesfahani & MacKinnon (1991), who reported that forcing shifts the predominant concentration towards the high-speed stream. These differences may be attributed to the effect of the forcing frequency. Koochesfahani & MacKinnon forced the flow well below its natural frequency, thus inducing subharmonic interactions and possible pairings, while in the present experiments the flow was forced slightly above the natural frequency. Although figure 5 shows an overall increase in mixing, the images of instantaneous temperature distributions (e.g. figure 5*c*) suggest that the mixed fluid was primarily concentrated around the periphery of the spanwise vortices and that there was a substantial amount of unmixed fluid within their cores.

The effects of spanwise-non-uniform forcing are shown in figures 6–8. Nygaard & Glezer (1991) reported that this form of forcing introduces packets of counter-rotating streamwise vortices that are similar to lambda vortices in flat-plate boundary layer flows. These vortices are formed downstream of the trailing edge of the flow partition and result in a substantial increase in small-scale motions within the shear layer. In the present experiment, the 'head' of each lambda vortex was formed near the high-speed edge of the primary vortices at spanwise locations that correspond to heaters that were operated at 4% power. The two counter-rotating legs of each lambda vortex resided within the braids region. Adjacent (counter-rotating) streamwise vortices merged into 'tails' near the low-speed edge of the upstream spanwise vortex. The effect of the lambda vortices on the mixing was assessed by measurements at three spanwise positions corresponding to the 'head' (Z_h, figure 6), the 'tail' (Z_t, figure 7), and the midpoint between Z_h, and Z_t (Z_{h-t}, figure 8).

As shown in earlier investigations, the interaction of the streamwise vortices with the primary (spanwise) vortices leads to the appearance of three-dimensional, small-scale motions around the periphery of the primary vortices and ultimately within their cores (e.g. Huang & Ho 1990; Nygaard & Glezer 1991). Furthermore, the streamwise vortices also induce the advection of low-speed fluid into the high-speed stream near the 'head' of the lambda vortex and, concomitantly, the advection of high-speed fluid into the low-speed stream near the 'tail'. In the present experiments, the streamwise vortices began to form at $Rx/\lambda_0 = 2.40$ and their presence had a profound effect on the cross-stream distributions of temperature. To begin with, it is apparent from distributions of the time-averaged temperature that more high- and low-temperature fluid was entrained into the shear layer in the cross-stream planes Z_h and Z_t (figures 6*a* and 7*a*, respectively) than in the unforced flow (figure 4*a*). In particular, in the plane Z_t (figure 7*a*), the flow was dominated by high-speed (i.e. low-temperature) fluid compared to the plane Z_h, indicating strong induced motion of high-speed fluid between adjacent counter-rotating streamwise vortices. The corresponding instantaneous temperature distributions $\theta(Y, t)$ suggest that the interaction between the spanwise and streamwise vortices altered the cores of the former (cf. Nygaard & Glezer 1991) and acted primarily to bring high-speed fluid towards the low-speed side of the shear layer. In the plane Z_{h-t}, $\theta(Y, t)$ shows both the spanwise vortex and a cross-section of the streamwise vortex (marked with an arrow in figure 8*a*).

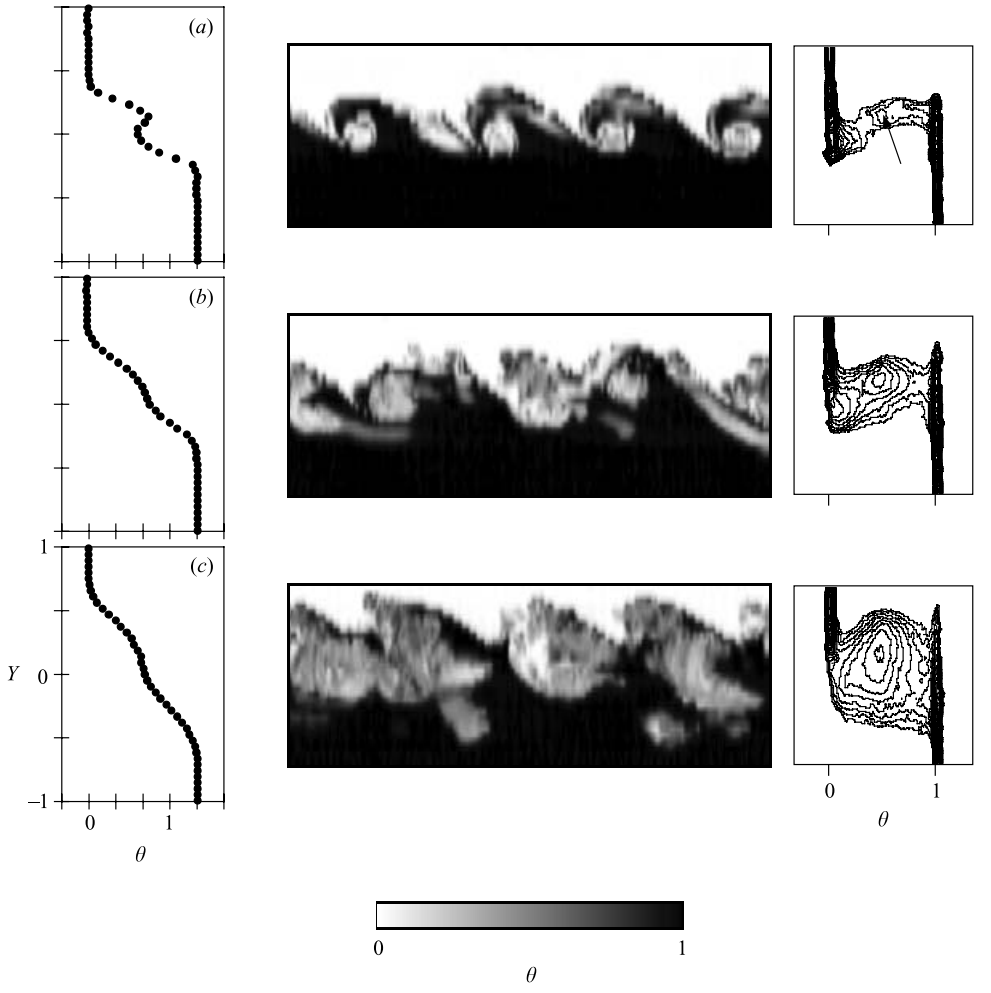

FIGURE 6. $\theta(Y)$, $\theta(Y,t)$, and p.d.f.(θ, Y) for SP forcing at $f = 6\,\mathrm{Hz}$ (Z_h) at (a) $Rx/\lambda_0 = 2.40$, (b) 3.60, and (c) 4.80. The contours of $\log_{10}(\text{p.d.f.}(\theta, Y))$ begin at a minimum level of -0.523 with a contour increment of 0.1.

Contour plots of p.d.f.(θ, Y) show a strong increase in mixing in the plane Z_h (figure 6*a*) compared to the unforced and the spanwise-uniform forced flow. Of particular note is the peak in p.d.f.(θ, Y) at $Rx/\lambda_0 = 2.40$ (see the arrow in figure 6*a*). This peak, at $\theta = 0.47$, was not present in figure 5(*a*) and can be attributed to mixing that was induced by the interaction between the primary and streamwise vortices near the high-speed edge of the shear layer. Such a peak was not present in the corresponding p.d.f. at Z_t in figure 7(*a*), presumably because the streamwise vortices develop fastest at the head and slowest at the tail. The peak in the p.d.f. was still present at $Rx/\lambda_0 = 3.60$ (figure 6*b*), and appeared to broaden in θ and Y farther downstream. By $Rx/\lambda_0 = 4.80$ (figure 6*c*), the peak encompassed a large portion of the p.d.f.(θ, Y) map, which indicates a wide region of mixed fluid within the shear layer covering a broad range of temperatures. This mixing may be attributed to the enhancement of small-scale motion, which is particularly apparent in images of $\theta(Y,t)$ in figure 6(*b*, *c*).

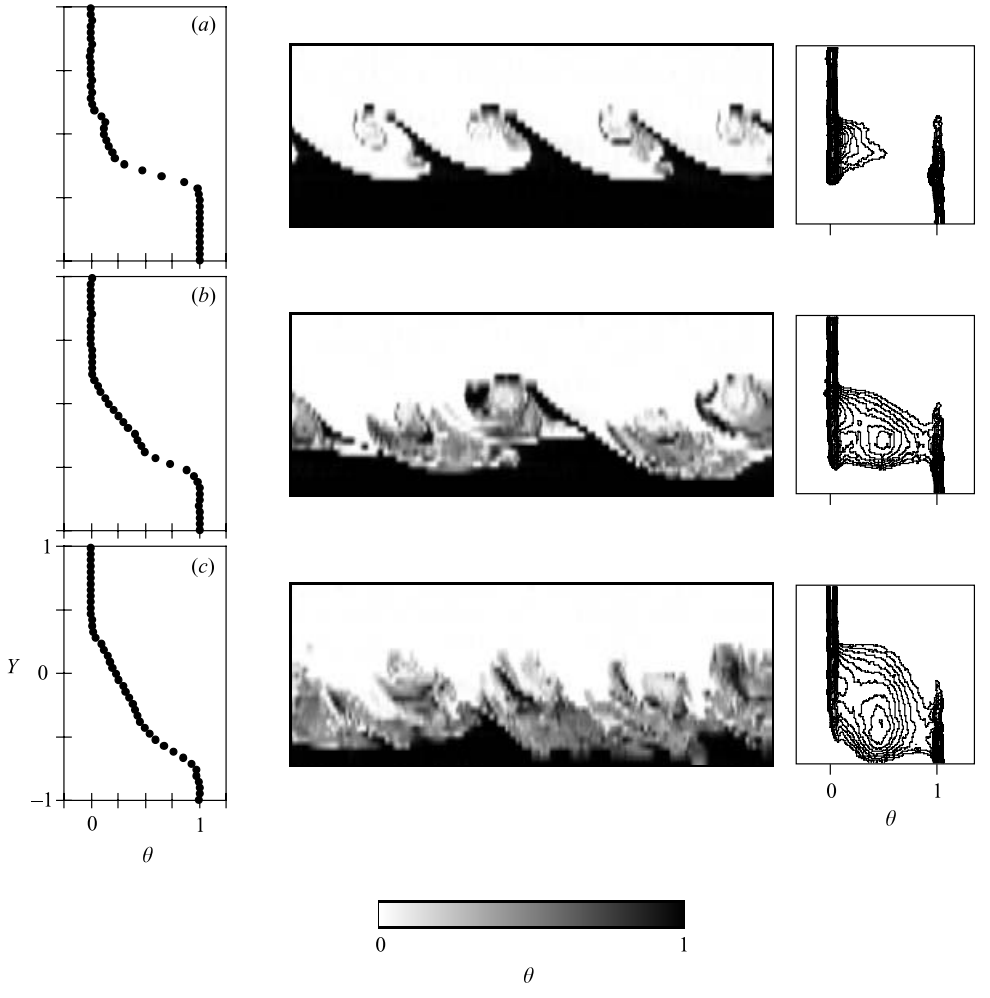

FIGURE 7. $\theta(Y)$, $\theta(Y,t)$, and p.d.f.(θ, Y) for SP forcing at $f = 6\,\mathrm{Hz}$ (Z_t) at (a) $Rx/\lambda_0 = 2.40$, (b) 3.60, and (c) 4.80. The contours of $\log_{10}(\text{p.d.f.}(\theta, Y))$ begin at a minimum level of -0.523 with a contour increment of 0.1.

The mixing near the plane $Z = Z_t$, (figure 7) was significantly affected by the cross-stream motion of high-speed fluid that is induced by the streamwise vortices. Plane shear layers typically entrain an excess of fluid from the high-speed stream (Dimotakis 1986, 1989) and the advection of high-speed fluid near the planes Z_t further increases the ratio of high-speed to low-speed fluid. As is evidenced from plots of $\theta(Y,t)$, the stirring motions induced by the streamwise vortices ensured that there is very little high-temperature fluid within the shear layer at all three streamwise stations in figure 7. The plots of p.d.f.(θ, Y), particularly at $Rx/\lambda_0 = 3.60$ and 4.80, reveal a 'plateau' of mixed fluid beginning at $\theta = 0$ and gradually rising to the peak at $\theta = 0.47$. However, at higher temperatures the amount of mixed fluid diminished sharply. Hence, most of the mixed fluid produced near the plane $Z = Z_t$ is at lower temperatures than near $Z = Z_h$ (figure 6) largely due to the lack of entrained hot fluid (from the low-speed side) at this spanwise position.

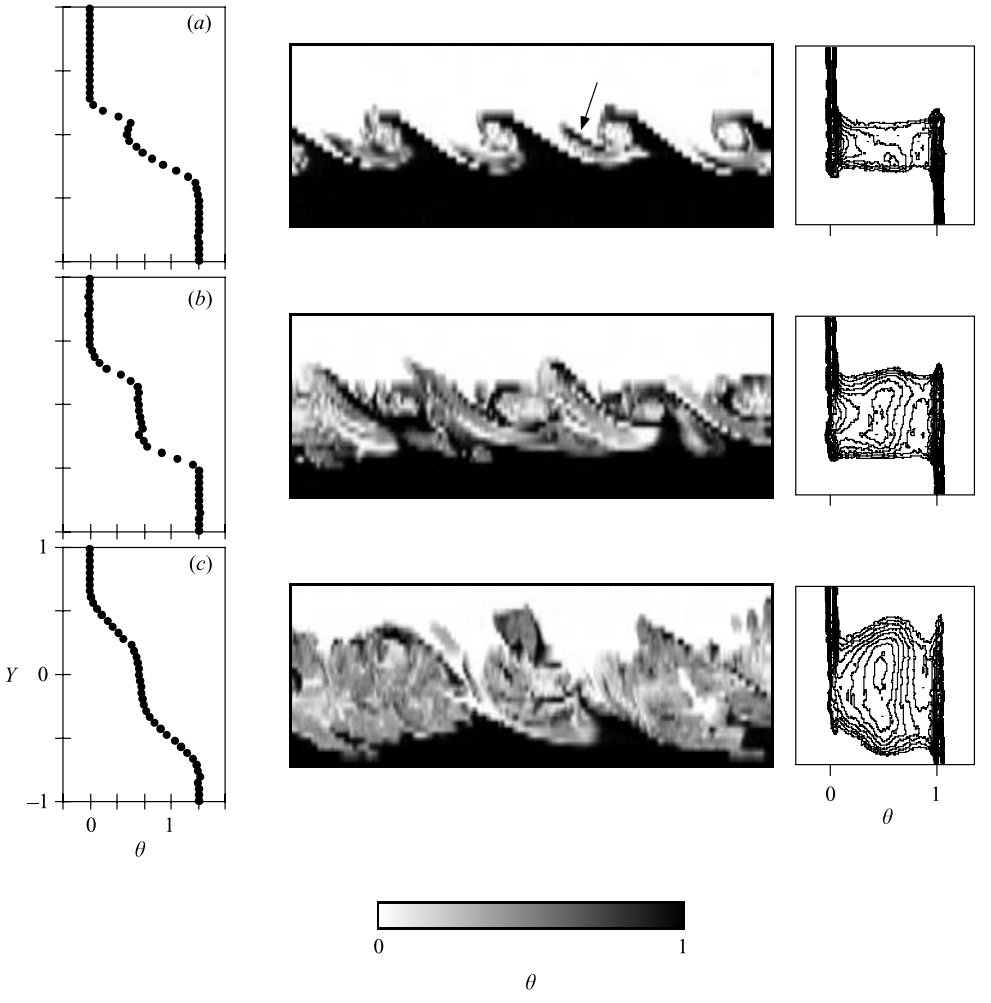

FIGURE 8. $\theta(Y)$, $\theta(Y, t)$, and p.d.f.(θ, Y) for SP forcing at $f = 6$ Hz (Z_{h-t}) at (*a*) $Rx/\lambda_0 = 2.40$, (*b*) 3.60, and (*c*) 4.80. The contours of $\log_{10}$(p.d.f.(θ, Y)) begin at a minimum level of -0.523 with a contour increment of 0.1.

As is evident from the contour plots of p.d.f.(θ, Y) in figure 8, the increase in mixing (compared to the unforced flow) was higher in cross-stream planes that intersect the legs of the streamwise vortices (nominally halfway between the 'head' and the 'tail') than at any other spanwise position. In fact, images of $\theta(Y, t)$ show both the spanwise vortex and a cross-section of the streamwise vortex (see arrow). By $Rx/\lambda_0 = 3.60$ (figure 8*b*), virtually the entire layer contained mixed fluid from either the spanwise vortex or the streamwise vortex, and the peak of p.d.f.(θ, Y) at $\theta = 0.47$ occurs over a significantly broader cross-stream domain than at the other two spanwise positions. By $Rx/\lambda_0 = 4.80$, there was a large amount of mixed fluid throughout the layer, although it was somewhat more concentrated at low temperatures, as was the case at the tail of the streamwise vortex.

As noted by earlier investigators, small characteristic spatial scales that are induced by straining of thin sheets of fluid or small-scale three-dimensional motions within the primary and secondary vortices are necessary for diffusion processes and molecular

mixing. Comparison of instantaneous temperature profiles $\theta(Y, t_i)$ for the unforced and spanwise-uniformly forced ($f = 6$ Hz) flows (figures 4 and 5, respectively) show how strained fluid layers lead to better mixing. The structure of small-scale motions is assessed from power spectra of turbulent temperature fluctuations, $S_T(\nu)$ (where ν is the non-dimensional frequency, $\nu = f/(6\,\text{Hz})$. Figure 9 shows $S_T(\nu)$ measured at the centreline of the shear layer ($Y = Z = 0$) at $X = 1.80$ (*a–c*), 3.60 (*d–f*), and 5.40 (*g–i*). There are three groups of spectral data: the unforced flow (a, d, g), SU at $f = 6$ Hz (b, e, h), and SP at $f = 6$ Hz (head) (c, f, i). The power spectra S_T are presented in a logarithmic form using an arbitrary unit system, and the curve for the unforced flow is repeated for reference with the data for SU and SP. Comparison between the power spectra of the unforced flow and its SU at $f = 6$ Hz counterpart shows an upstream increase in small-scale motions ($\nu \geqslant 1$) in the forced flow. There was little apparent difference at $X = 5.40$, however. By contrast, SP forcing greatly increased the amount of small-scale motion at all streamwise stations. The difference was particularly dramatic at $X = 1.80$ (figure 9*c*); however, this increase in small-scale motion was apparent at $X = 3.60$ (figure 9*f*) and $X = 5.40$ (figure 9*i*) as well.

When the shear layer was simultaneously forced at a fundamental frequency of 7.7 Hz and its subharmonic 3.85 Hz, controlled pairing of the primary vortices was induced. The pairing process was accompanied by an increase in entrainment and the layer width δ. Figure 10 shows the effect of controlled pairing on the mixing. The temperature distribution $\theta(Y, t)$ shows that the primary vortices began to pair at $X = 2.40$ (figure 10*a*). The pairing process continued through $X = 3.60$ (figure 10*b*) and was complete at $X = 4.80$ (figure 10*c*), where the passage frequency of the vortical structures was 3.85 Hz. This pairing of the primary vortical structures resulted in layer widths of $\delta = 2.74$ cm, 4.17 cm, and 6.05 cm at $X = 2.40$, 3.60, and 4.80, respectively. These values compare with $\delta = 2.63$ cm, 3.71 cm, and 5.38 cm at the same streamwise stations for SU at $f = 6$ Hz – an increase of approximately 12% at the two downstream stations. Perhaps more surprising was the fact that there was a significant increase in small-scale motion within engulfed vortices as the pairing process occurred (see arrow in figure 10*b*). As the vortices paired, the thin layers collapsed together, until finally the paired vortex was filled with mixed fluid (figure 10*c*). Comparisons of p.d.f.(θ, Y) at $X = 3.60$ and $X = 4.80$ for this case with its SU counterpart show substantially more mixing in the pairing case. Particularly noticeable is the peak at $\theta = 0.17$ which was not present in the case of SU at $f = 6$ Hz.

A plot of the integral performance measure, PM, is presented as a function of the pairing parameter $X = Rx/\lambda_0$ in figure 11. Figure 11(*a*) shows PM(X) for the unforced flow and confirms that there was very little mixed fluid until approximately $X = 2.36$, where the flow began to undergo mixing transition. The figure also shows that by $X = 5.40$, PM(X) had reached a value of 0.088, almost an order of magnitude higher than at $X \leqslant 2.36$. This is in accordance with the findings of Konrad (1976) and Roberts & Roshko (1985).

Figure 11(*b*) shows the change in PM, ΔPM, at each streamwise station for SU and SP forcing at $f = 6$ Hz, relative to the unforced case. Curves are shown at the head (Z_h), the tail (Z_t), and the midpoint section (Z_{h-t}) of the streamwise vortex. It is apparent that both forms of forcing effected a maximum increase in PM between approximately $X = 1.88$ and $X = 2.84$. In the case of SU, for example, ΔPM reaches a maximum of approximately 0.37 (37% above the unforced level) at $X = 2.10$, whereas in the case of SP forcing ΔPM reaches a maximum of between 1.50 and 3.00 (150% to 300% above the unforced level) depending on the spanwise position. The level of ΔPM is highest at Z_{h-t}, as would be expected from the p.d.f. data in figure 8. This

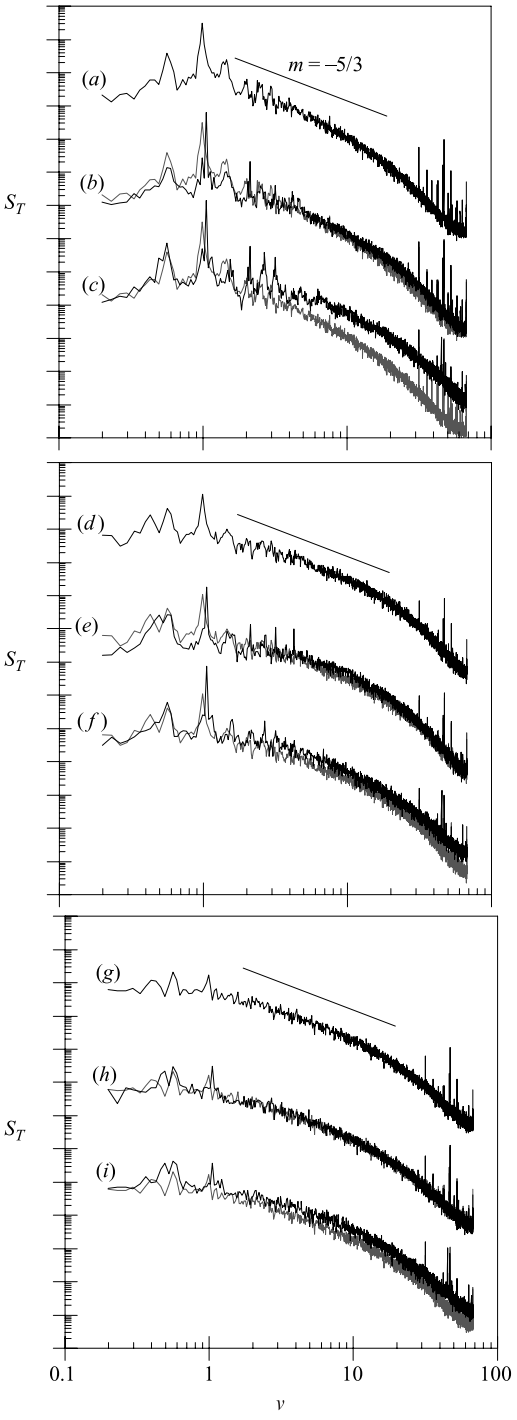

FIGURE 9. Spectra of temperature variance S_T at (*a–c*) $Rx/\lambda_0 = 1.80$, (*d–f*) 3.60, and (*g–i*) 5.40. Shown are the unforced flow (*a*, *d*, *g*), SU forcing at $f = 6$ Hz (*b*, *e*, *h*), and SP forcing at $f = 6$ Hz (head) (*c*, *f*, *i*). Data are measured at $Y = Z = 0$. The curves for SU and SP forcing also show the corresponding unforced case in grey.

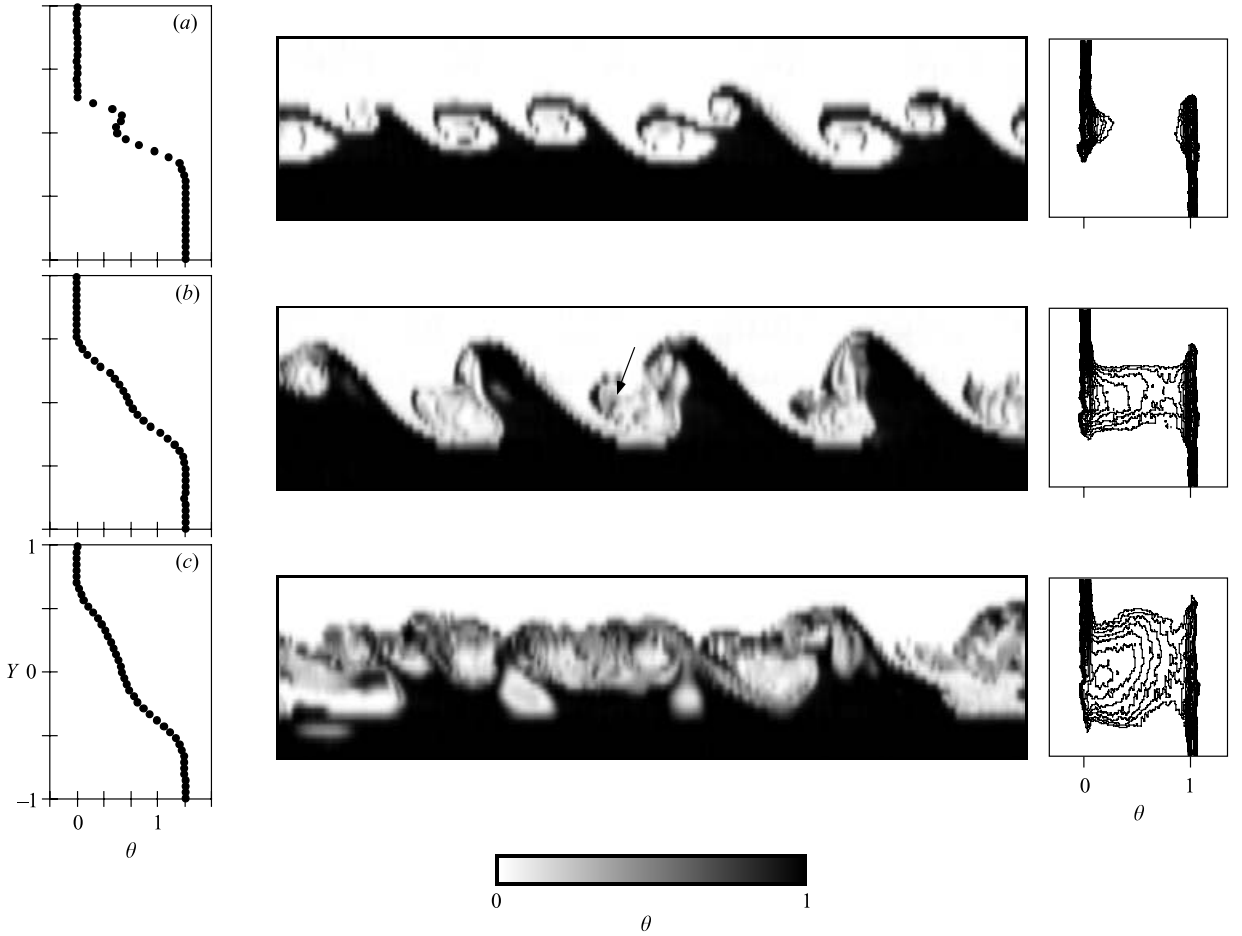

FIGURE 10. $\theta(Y)$, $\theta(Y, t)$, and p.d.f.(θ, Y) for SU forcing at $f = 3.85$ and 7.7 Hz at (*a*) $Rx/\lambda_0 = 2.40$, (*b*) 3.60, and (*c*) 4.80. The contours of $\log_{10}$(p.d.f.(θ, Y)) begin at a minimum level of -0.523 with a contour increment of 0.1.

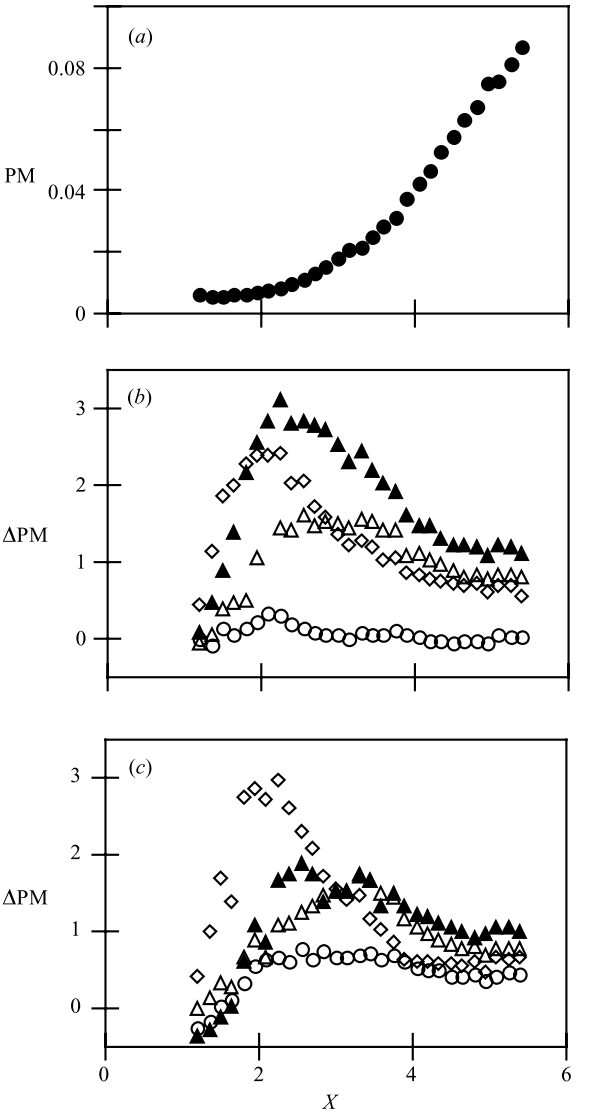

FIGURE 11. (*a*) PM(X) for the unforced flow; (*b*) ΔPM for SU at $f = 6$ Hz (○), and SP at $f = 6$ Hz (Z_h) (◇), (Z_t) (△), and (Z_{h-t}) (▲), (*c*) ΔPM for SU at $f = 3.85$ and 7.7 Hz (○), and SP at $f = 3.85$ and 7.7 Hz (Z_h) (◇), (Z_t) (△), and (Z_{h-t}) (▲).

high level of mixing is due to the fact that at this station, mixed fluid from the cores of both the spanwise and the streamwise vortices was measured. Note that these findings are much higher than the 22% increase in mixed fluid reported by Koochesfahani & MacKinnon (1991) using a spanwise-uniform skewed-harmonic waveform.

The two-wave configuration of SU forcing with $f = 3.85$ and 7.7 Hz significantly increased PM relative to its single-wave counterpart at $f = 6$ Hz. For multi-frequency forcing, $\Delta\text{PM} \approx 0.50$ at all streamwise stations for $X \geqslant 2.0$, whereas for single-frequency SU forcing ΔPM was positive only for $1.00 \leqslant X \leqslant 2.50$. Although pairing enhanced mixing, and SP forcing enhanced mixing, in combination they interacted unfavourably. The configuration of SP at $f = 3.85$ and 7.7 Hz resulted in overall lower

values of ΔPM than did SP at $f = 6$ Hz. At the tail of the streamwise vortex, the values of ΔPM are similar for single-frequency and multi-frequency forcing. At the head of the streamwise vortex, the levels of ΔPM are slightly higher at upstream locations for SP at $f = 3.85$ and 7.7 Hz, but slightly lower at downstream locations. The most dramatic difference is at Z_{h-t}, where ΔPM is significantly greater for SP at $f = 6$ Hz than for SP at $f = 3.85$ and 7.7 Hz. This suggests that the pairing process reduced the strength of the streamwise vortices in downstream locations and diminished their effective mixing power. This notion accords with the work of Moser & Rogers (1993), who observed that pairing reduces the growth of three-dimensionality of the vortical structures.

An interesting observation on the effect of the forcing with downstream distance can be obtained from figures 11(*b*) and 11(*c*): although the unforced mixing transition is not complete by the end of the test section, and thus the effect of the forcing on mixing past the mixing transition is not completely known, the effect of forcing remains strong throughout most of the mixing transition region itself. In fact, the streamwise variation of ΔPM (the relative increase in mixing as a result of the forcing) levels off and shows no sign of decreasing at the end of the test section ($X = 5.40$).

Further insight into the mixing process may be attained from moments of p.d.f.(θ, Y):

(*a*) the total mixed fluid in the layer, M^0, is defined by

$$M^0 = \int_{\varepsilon}^{1-\varepsilon} \int_{-\infty}^{+\infty} \text{p.d.f.}(\theta, Y)\, \mathrm{d}Y\, \mathrm{d}\theta$$

and is non-dimensional, since Y is non-dimensional;

(*b*) the average temperature of mixed fluid within the layer, θ_c, is defined by

$$\theta_c \equiv M_T^1 = \frac{1}{M^0} \int_{\varepsilon}^{1-\varepsilon} \int_{-\infty}^{+\infty} \theta\, \text{p.d.f.}(\theta, Y)\, \mathrm{d}Y\, \mathrm{d}\theta;$$

(*c*) the average cross-stream position of mixed fluid within the layer, Y_c, is defined by

$$Y_c \equiv M_Y^1 = \frac{1}{M^0} \int_{\varepsilon}^{1-\varepsilon} \int_{-\infty}^{+\infty} Y\, \text{p.d.f.}(\theta, Y)\, \mathrm{d}Y\, \mathrm{d}\theta.$$

Figure 12 shows moments of p.d.f.(θ, Y) for unforced SU at $f = 6$ Hz, and SP at $f = 6$ Hz, at Z_h, Z_t, and Z_{h-t}. The trends of M^0 in figure 12(*a*) appear similar to those of PM(X), implying that the integral performance measure introduced in the current work is as good a descriptor as the total mixed fluid in quantifying the degree of mixing, and may be compared to other works which use the latter. As expected, the values of M^0 were significantly higher in the case of SP forcing than in the case of SU forcing, particularly at Z_{h-t}. Figure 12(*b*) presents the average temperature of mixed fluid in normalized form. The plots for both the unforced flow and the SU case show a decrease in average mixed fluid temperature from $X = 2.40$ to $X = 5.40$. This finding that θ_c for the unforced flow shifted towards the high-speed concentration with downstream distance is at odds with the results of Koochesfahani & Dimotakis (1986). They found that the average concentration shifts towards the low-speed concentration, and attribute this to excess entrainment of high-speed fluid into the vortex region during the initial rollup. However, the predicted θ_c (from Dimotakis' 1986, 1989 entrainment ratio argument) is 0.43, close to the values seen around $X = 3.00$ (although θ_c decreases with downstream distance). By contrast, the mixed fluid temperature at all three SP spanwise locations increased with streamwise

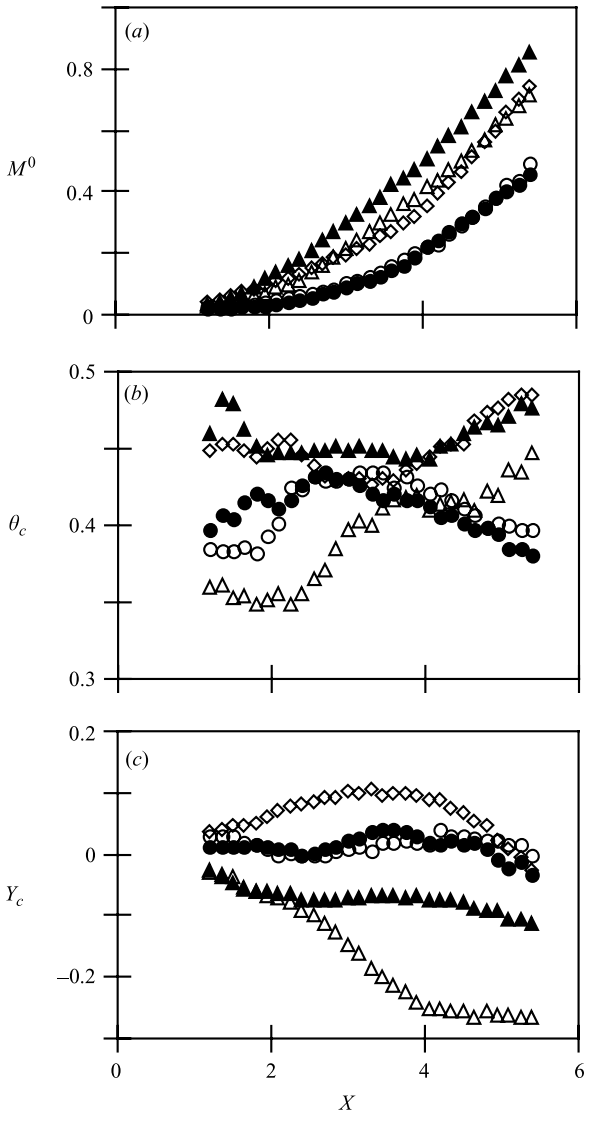

FIGURE 12. (*a*) Total mixed fluid M^0; (*b*) average temperature of mixed fluid θ_c, and (*c*) average cross-stream position of mixed fluid Y_c for unforced (●), SU at $f = 6$ Hz (○), SP at $f = 6$ Hz (Z_h) (◇), SP at $f = 6$ Hz (Z_t) (△), and SP at $f = 6$ Hz (Z_{h-t}) (▲).

position, which is consistent with the simulations of Buell & Mansour (1989) in their spatially developing mixing layer. As a result of the pumping action of the counter-rotating streamwise vortices (which entrained hot, low-speed fluid into the layer at the head), the average mixed fluid temperature was higher at the head than at the tail of these structures.

Figure 12(*c*) shows the average cross-stream position of mixed fluid for these forcing configurations. Consistent with the pumping action, the Y_c values indicate upward displacement at the head, and downward displacement at the tail of the streamwise vortices. For the unforced and SU at flows $f = 6$ Hz, Y_c values varied by less than 0.04 about the geometric centre of the test section ($Y = 0$). For SP at $f = 6$ Hz forcing, Y_c

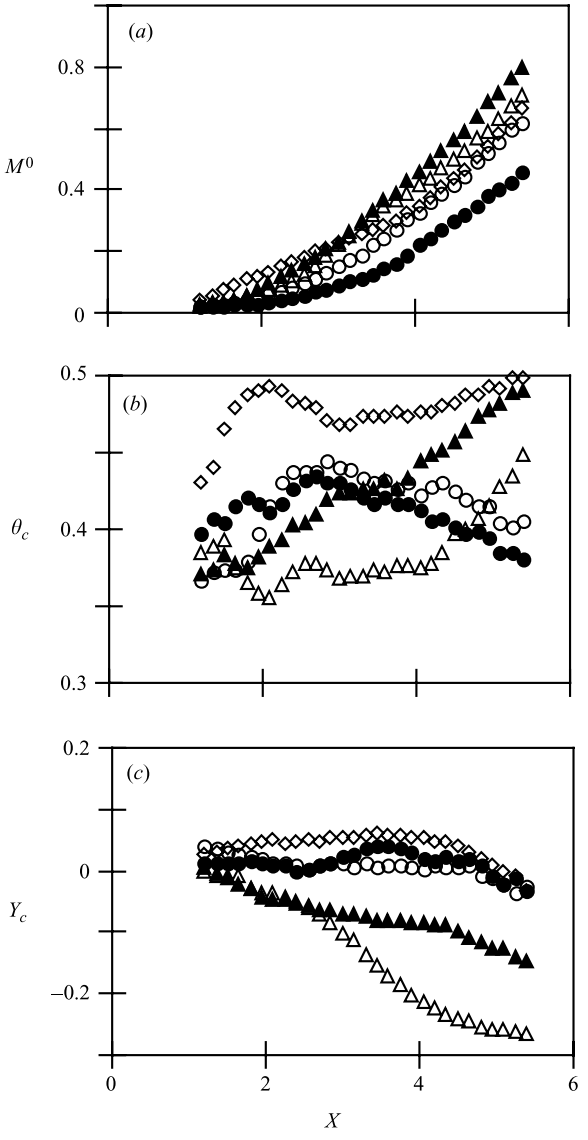

FIGURE 13. (*a*) Total mixed fluid M^0, (*b*) average temperature of mixed fluid θ_c, and (*c*) average cross-stream position of mixed fluid Y_c for unforced (●), SU at $f = 3.85$ and 7.7 Hz (○), SP at $f = 3.85$ and 7.7 Hz (Z_h) (◇), SP at $f = 3.85$ and 7.7 Hz (Z_t) (△), and SP at $f = 3.85$ and 7.7 Hz (Z_{h-t}) (▲).

began to decrease at the head and approach a constant value at the tail for $X \geqslant 4.00$, suggesting a weakening of the streamwise vortices.

Figure 13 shows the moments of p.d.f. for SU at $f = 3.85$ and 7.7 Hz and SP at $f = 3.85$ and 7.7 Hz. Also included in the figure for reference is the unforced flow. The total mixed fluid entry M^0 accords with the trend of PM(X), by showing a smaller difference between the SP cases and the SU case than in the case of single-frequency forcing at 6 Hz. As in the single-frequency case, the spanwise position Z_{h-t} had the highest values of M^0. The average mixed fluid temperature values, θ_c, for SU at $f = 3.85$ and 7.7 Hz appear to be similar to their single-frequency counterparts (and

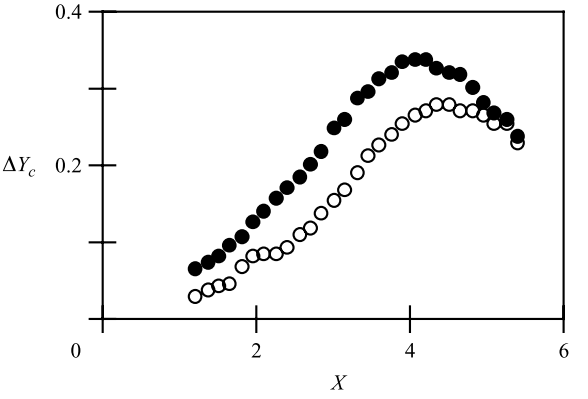

FIGURE 14. $\Delta Y_c(X)$ for SP at $f = 6$ Hz (●) and SP at $f = 3.85$ and 7.7 Hz (○).

to the unforced flow) at all streamwise stations. As was the case with the single-frequency SP waveform, forcing with SP at $f = 3.85$ and 7.7 Hz caused θ_c to increase with downstream distance at all three spanwise stations. In addition to increasing, the values of θ_c at the three spanwise positions became more uniform with downstream distance. By the end of the measurement domain, the values were within 0.05 of each other, compared to a difference of up to 0.15 at upstream locations. The SP case at $f = 6$ Hz was even more homogeneous across the span of the layer, with differences in θ_c of less than 0.05 for $X \geqslant 3.20$.

The average position of mixed fluid, Y_c, in the SU mode at $f = 3.85$ and 7.7 Hz was similar to its $f = 6$ Hz counterpart. However, for the SP mode at $f = 3.85$ and 7.7 Hz, Y_c was lower at the head and higher at the tail of the vortex than in the corresponding SP case at $f = 6$ Hz, suggesting that the streamwise vortices were weaker in the multiple-frequency forcing than in the case of SP at $f = 6$ Hz. This point can be further elaborated by comparing ΔY_c (the difference in the average location of mixing, Y_c, at the head and the tail) for the two cases. As the streamwise vortices increase Y_c at the head and decrease it at the tail of the streamwise vortex, ΔY_c is an indicator of the strength of the streamwise vortices. Figure 14 shows the streamwise variation of ΔY_c for SP at $f = 6$ Hz and SP at $f = 3.85$ and 7.7 Hz. It is apparent that at all streamwise stations the difference in Y_c was greater for single-frequency SP forcing than for its multiple-frequency counterpart. The flow was more three-dimensional in the former case due to the actions of the stronger streamwise vortices. The stronger streamwise vortices appear to be the reason why PM(X) is higher for SP at $f = 6$ Hz (particularly at Z_{h-t}) than for SP at $f = 3.85$ and 7.7 Hz.

Finally, plots of $\tilde{\delta}(X)$ (the width of the shear layer non-dimensionalized by λ_0/R) and of the mixed fluid fraction ($V_m = M^0/\tilde{\delta}$) can be used to determine whether mixing enhancement occurred due to increased layer width or increased molecular mixing. Figure 15(*a*) shows $\tilde{\delta}(X)$ for the unforced flow, in which the width of the layer increased linearly with downstream distance and reached a value of 1.48 at $X = 5.40$. Forcing with the SU mode at 6 Hz had a marginal effect on the width of the layer (figure 15*b*). It tended to decrease the layer width slightly at the downstream stations but had no apparent influence at the upstream locations. By contrast, the SP mode at $f = 6$ Hz increased the layer width. This outcome was expected since the streamwise vortices reside on the outside edges of the primary rollers. Although inducing pairing of the primary vortices by forcing at $f = 3.85$ and 7.7 Hz might be expected to significantly

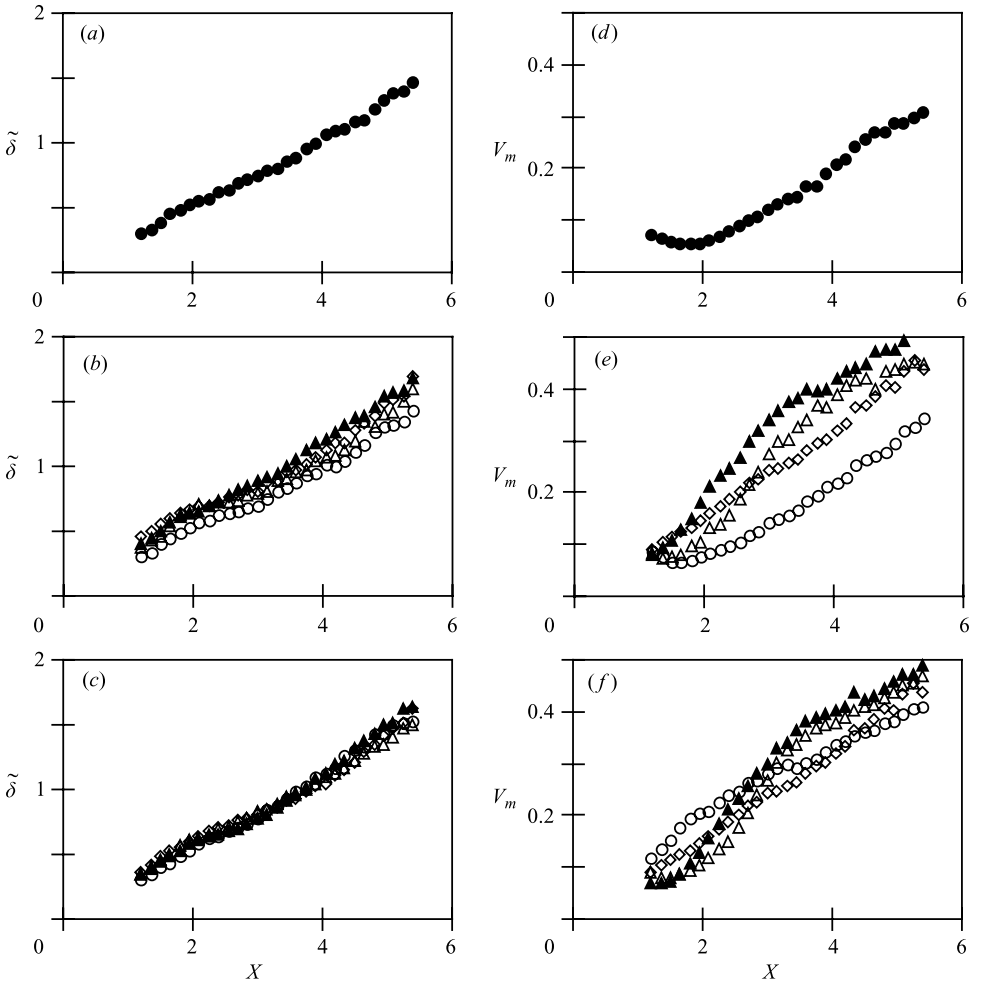

FIGURE 15. (*a–c*) Layer width $\tilde{\delta}(X)$ and (*d–f*) mixed fluid fraction $V_m(X)$, (*a*, *d*) for the unforced flow; (*b*, *e*) SU at $f = 6$ Hz (○), and SP at $f = 6$ Hz (Z_h) (◇), (Z_t) (△), and (Z_{h-t}) (▲); and (*c*, *f*) SU at $f = 3.85$ and 7.7 Hz (○), and SP at $f = 3.85$ and 7.7 Hz (Z_h) (◇), (Z_t) (△), and (Z_{h-t}) (▲).

increase the width of the layer, figure 15(*c*) shows that multiple-frequency SU forcing increased the width of the layer only slightly. In addition, since pairing inhibited the formation of the streamwise vortices, SP forcing at $f = 3.85$ and 7.7 Hz did not significantly enhance the width of the layer at any of the three spanwise positions either.

Koochesfahani & MacKinnon (1991) found that forcing increases mixing mainly by increasing layer width. Since forcing did not seem to increase the width of the layer in the present study, a different mechanism must have been responsible for the increased mixing. Figure 15(*d–f*) shows the mixed fluid fraction V_m for the unforced flow, $f = 6$ Hz forcing, and $f = 3.85$ and 7.7 Hz forcing, respectively. The unforced layer (figure 15*d*) was approximately 5% mixed for $X \leqslant 2.50$. Beyond this location, the mixed fluid fraction increased almost linearly to 0.32 at $X = 5.40$. Since V_m by definition must be $\leqslant 1.0$ (and other researchers (Pickett & Ghandhi 2001) have shown that it reaches an asymptotic value of approximately 0.5 in highly diffusive (gaseous)

layers), the fact that it was still increasing at the end of the test section implies that mixing transition was not complete. It is likely that for some value of $X > 5.40$, the mixed fluid fraction V_m levelled off and reached an asymptotic value and that mixing transition was completed.

Forcing with SU at $f = 6$ Hz tended to slightly increase the molecular mixing at all streamwise stations. This may be attributed to the tight winding of the thin laminar diffusion layers. Circulation in the shear layer is constant and determined solely by the velocity difference ΔU. Hence, small vortical structures may have a more concentrated vorticity distribution that leads to an increase in molecular mixing. However, further downstream, as the growth of the layer was reduced, the overall mixed fluid and PM were less than in the unforced case.

For SP forcing at $f = 6$ Hz, the mixed fluid fraction V_m was highest at Z_{h-t}. This suggests that as fluid was entrained into the streamwise vortices (which have a smaller cross-section than the spanwise vortices) the fluid was mixed immediately. Interestingly, V_m was lowest at the head of the streamwise vortex, suggesting that there was a large amount of additional free-stream fluid entrained at this spanwise position.

Induced pairing due to $f = 3.85$ and 7.7 Hz forcing increased the level of molecular mixing (figure 15*f*). The curves show that V_m increased at all streamwise stations, with the slope greatest for $2.00 \leqslant X \leqslant 4.00$. It is noteworthy that all four curves begin to level off at $X \approx 4.00$, indicating saturation. As was shown in figure 10, this is the region over which the pairing process occurred. Forcing with SP at $f = 3.85$ and 7.7 Hz actually decreased molecular mixing for $X \leqslant 3.00$ compared to the spanwise-uniform case. Far downstream, however, V_m was higher for the spanwise-periodic case than for its SU counterpart.

5. Phase-averaged measurements

Given the intermittent nature of the plane shear layer, it is clear that mixing in this flow varies significantly with space and time. The present results demonstrate that most of the mixing occurs within the primary and secondary vortices. In focusing on the shear layer during time-harmonic forcing, where the flow is phase-locked to the forcing signal, it is possible to obtain information on the phase-averaged mixing that is directly related to the topological features of the vortical structures. In addition, comparisons can be made among the various forcing configurations. To this end, data were sampled phase-locked to the forcing signal at a sampling rate of 128 points per cycle for the $f = 6$ Hz cases and at 128 points per low-frequency (3.85 Hz) cycle in the $f = 3.85$ and 7.7 Hz cases. Over 300 cycles were obtained and the resulting signals were phase-averaged to properly quantify the flow during a representative cycle. Time is non-dimensionalized as $\tau = t/T_f$, where T_f is the period of the forcing cycle (167 ms or 260 ms). All phase-averaged quantities are denoted with angle brackets, i.e. $\langle\theta(Y, \tau)\rangle$ is phase-averaged $\theta(Y, t)$. Data taken at different measurement stations can be combined to reconstruct the flow field as a function of three spatial dimensions and time, i.e. $\langle\theta(X, Y, Z, \tau)\rangle$.

5.1. *Topology of the mixing structures*

Further insight into the mixing process was obtained by considering its progress as a function of spatial (and particularly spanwise) position in the layer. The flow field in (Y, Z)-planes was reconstructed from phase-locked measurements. The forcing modes

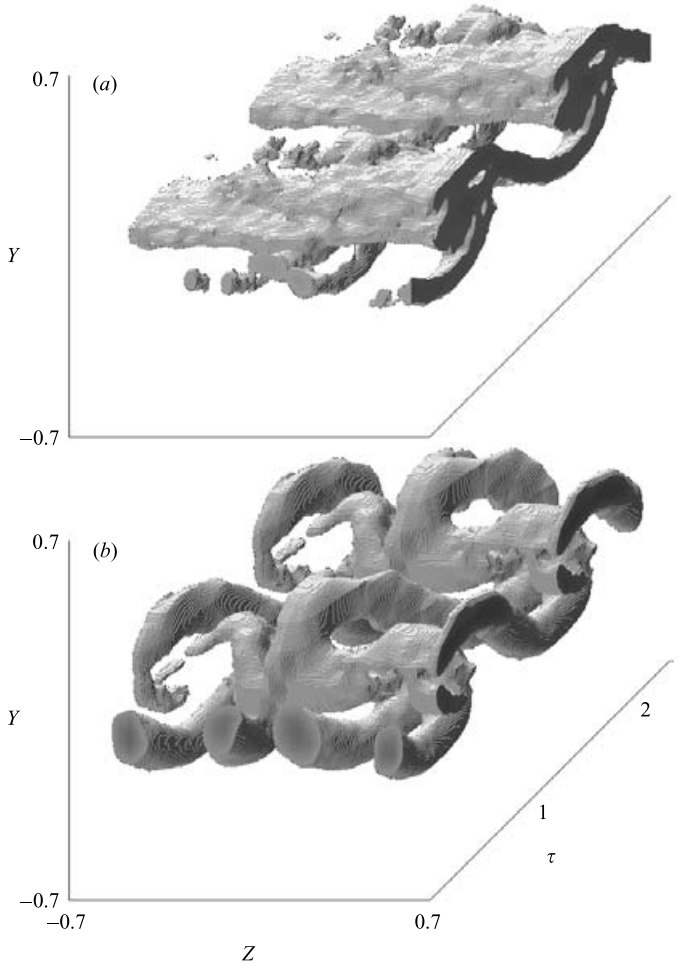

FIGURE 16. Phase-averaged $\langle \text{p.m.}(Y, Z, \tau)\rangle$ for (*a*) SU at $f = 6$ Hz and (*b*) SP at $f = 6$ Hz at $Rx/\lambda_0 = 2.40$.

were SU and SP at $f = 6$ Hz, with a spanwise wavelength of $Z = 0.62$ and duty cycle of 75% in the SP case.

Figure 16(*a*, *b*) presents isosurface plots of the phase-averaged performance measure $\langle \text{p.m.}(X, Y, \tau)\rangle$ for (*a*) SU and (*b*) SP at $X = 2.40$. The Y and Z coordinates represent the cross-stream (vertical) and spanwise (horizontal) planes, respectively, and the time coordinate is directed into the plane of the page. The phase in the forcing cycle has been shifted for convenience in viewing the structure of the flow. Two periods of the excitation waveform and two wavelengths of the spanwise waveform are shown. The reference box is a volume consisting of a 0.70×0.70 grid in the (Y, Z)-plane and a length in the time dimension that is scaled with the convection velocity. The level of p.m. is graded from 0 (white) to 0.25 (black), where the latter indicates fully mixed fluid at the mean temperature of the two free streams. The same greyscale was maintained in both parts of the figure, but, to accentuate certain features of the flow, the isosurface transparency level was chosen on a case-by-case basis: 0.05 for the SU case and 0.08 for the SP case.

Upstream of the mixing transition there was very little mixed fluid within the cores of the primary (spanwise) vortices, but the streamwise vortices in the SP case induced substantial mixing. Indeed, the fluid in the centre of these vortices was almost completely mixed – although the volume over which this process took place was quite small. By contrast, there was very little mixing in the SU case. Although most of the mixing that was present occurred in the cores of the primary vortices, a small amount of mixed fluid was present in naturally occurring streamwise vortices. There was significant three-dimensionality to the structure of the flow, even though it was forced with a two-dimensional waveform. This reinforces the idea that mixing is by its nature a three-dimensional phenomenon.

5.2. *Mixed fluid composition*

Because data were acquired phase-locked to the forcing signal, measures of mixed fluid composition could be calculated in different parts of the layer and at different phases in a representative cycle. Figures 17–20 show composite plots for SU and SP at $f = 6$ Hz, and at $f = 3.85$ and 7.7 Hz, respectively. The spanwise position for the SP data was the head of the streamwise vortex (Z_h). The data are presented at one streamwise station, $X = 3.60$, which was well within the natural mixing transition region, and where the primary rollers were beginning to pair when forced with the multiple-frequency waveforms.

The top row of each figure presents the phase-averaged probability density function of temperature $\langle \text{p.d.f.}(\theta, Y; \tau_i)\rangle$ at four representative points in a phase. These contour plots provide a measure of the composition and total mixed fluid in different parts of the layer as a function of phase in the forcing cycle. Below the contour plots are raster images of two cycles of the phase-averaged (a) temperature $\langle \theta(Y, \tau)\rangle$ and (b) mixed fluid temperature $\langle \theta_{mixed}(Y, \tau)\rangle$ with the times corresponding to the contour plots indicated. Clearly, $\theta_{mixed}(Y) \neq \theta(Y)$ because unmixed fluid from the free streams is not considered in the θ_{mixed} average. The mixed fluid temperature provides a convenient way of checking the existence of 'marching' p.d.f.s, an issue that has been debated extensively over the years (Batt 1977; Konrad 1976). Inclusion of this measure also permits direct comparison of the current results with the numerical findings of Park, Metcalfe & Hussain (1994) as well as the experimental research of Koochesfahani & Dimotakis (1986). Finally, each composite presents in (c) the phase-averaged mixed fluid, $\langle M^0(\tau)\rangle$, and in (d) layer-averaged mixed fluid temperature $\langle \theta_c(\tau)\rangle$. These two quantities are the phase-averaged versions of the time-averaged data shown in figures 12(a, b) and 13(a, b).

Figure 17 presents $\langle \text{p.d.f.}(\theta, Y; \tau_i)\rangle$ data for $\tau = 0.016$, 0.266, 0.516, and 0.766, respectively, for SU at $f = 6$ Hz. It is apparent that the SU mode led to very little mixing within the braids region and, therefore, much of the activity remained confined to a region within the primary vortex. This mixing occurred when the thin diffusion layers collapsed around the periphery of the spanwise roller. The probability density $\langle \text{p.d.f.}(\theta, Y; \tau_i)\rangle$ at the beginning (τ_3), through the centre (τ_4), and at the end (τ_1) of the spanwise roller shows mixed fluid being produced at all temperatures, although weighted towards the high-speed (low) temperature. The time τ_4 exhibits the greatest amount of mixing, but, as the p.d.f. shows, this mixing occurred not at the centre of the spanwise vortex but mostly at its high-speed side. As shown in the plot of $\langle M^0(\tau)\rangle$, the amount of mixed fluid varied almost sinusoidally, with a maximum of 0.24 at τ_4 in the core region and a minimum of 0.08 at τ_2 in the braids region. The time average of $\langle M^0(\tau)\rangle$ is 0.16, as was previously shown in figure 12(a).

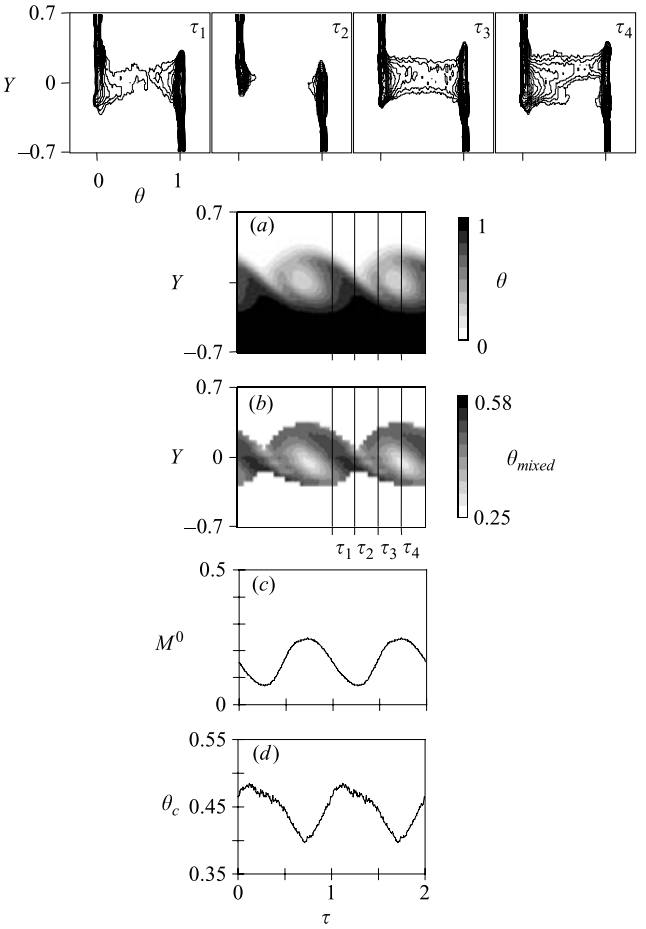

FIGURE 17. Top: $\langle \text{p.d.f.}(\theta, Y; \tau_i)\rangle$ at times $\tau = 0.016$, 0.266, 0.516, and 0.766; (*a*) $\langle \theta(Y, \tau)\rangle$, (*b*) $\langle \theta_{mixed}(Y, \tau)\rangle$, (*c*) $\langle M^0(\tau)\rangle$, and (*d*) $\langle \theta_c(\tau)\rangle$, for SU at $f = 6$ Hz. Data are measured at $Rx/\lambda_0 = 3.60$. The contours of $\log_{10}(\langle \text{p.d.f.}(\theta, Y; \tau_i)\rangle)$ begin at a minimum level of -0.523 with a contour increment of 0.1.

The image of $\langle \theta_{mixed}(Y, \tau)\rangle$ (figure 17*b*) shows that there was an 'island' of cool mixed fluid at the centre of the spanwise vortices, surrounded by warmer fluid. A possible explanation of this finding is that fluid which is entrained into the core of the spanwise vortex mixed at a temperature controlled by the large-scale entrainment ratio, while fluid in the braids region mixed at a temperature much closer to the mean temperature of the free streams. The layer-averaged mixed fluid temperature $\langle \theta_c(\tau)\rangle$ (figure 17*d*) had a minimum value of 0.40 in the core region, very close to what would be expected from the estimated entrainment ratio based on the arguments of Dimotakis (1986, 1989), (0.43). The maximum of $\langle \theta_c(\tau)\rangle$ occurred in the braids region, with a value of 0.48.

Figure 18 presents phase-averaged data for the SP forcing mode at $f = 6$ Hz, at the head position of a streamwise vortex. A peak in the p.d.f. at $Y \approx 0.24$ and $\theta \approx 0.47$ is visible at times τ_3 and τ_4. Clearly, the streamwise vortex was responsible for the fluid being mixed at these intermediate temperatures in this forcing configuration since this peak was not present in the SU case. Comparison between the SU and SP cases shows that both produced mixed fluid at a low temperature (e.g. at time τ_4) in the

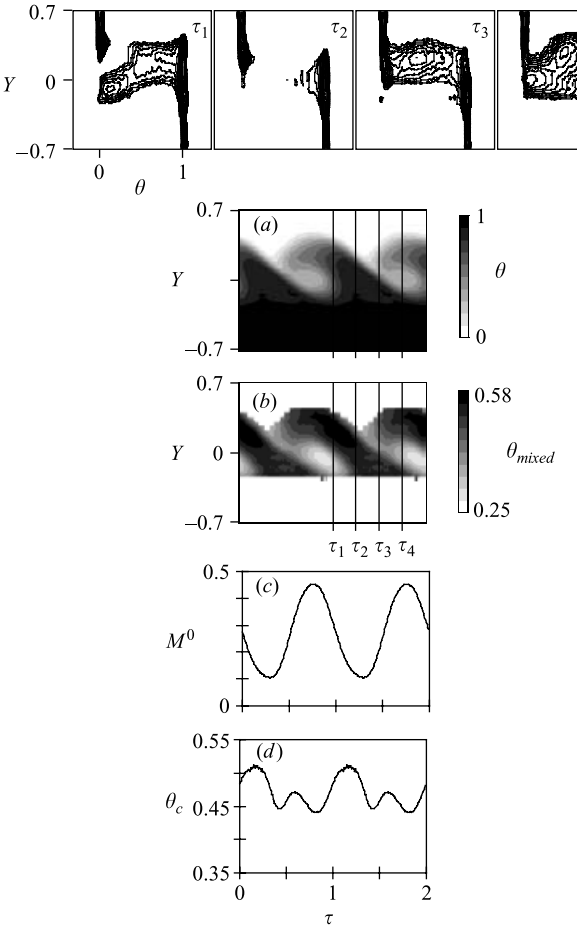

FIGURE 18. Top: $\langle \text{p.d.f.}(\theta, Y; \tau_i)\rangle$ at times $\tau = 0.016$, 0.266, 0.516, and 0.766; (*a*) $\langle \theta(Y, \tau)\rangle$, (*b*) $\langle \theta_{mixed}(Y, \tau)\rangle$, (*c*) $\langle M^0(\tau)\rangle$, and (*d*) $\langle \theta_c(\tau)\rangle$, for SP at $f = 6$ Hz (Z_h). Data are measured at $Rx/\lambda_0 = 3.60$. The contours of $\log_{10}(\langle \text{p.d.f.}(\theta, Y; \tau_i)\rangle)$ begin at a minimum level of -0.523 with a contour increment of 0.1.

core of the primary vortex. The maximum in $\langle M^0(\tau)\rangle$ occurred at approximately the same point in phase as in the SU case, τ_4, corresponding to the temporal centre of the spanwise vortex. In the SP case, however, the maximum value $\langle M^0(\tau)\rangle$ was 0.46, compared with 0.24 in the SU case.

Figure 18(*b*) shows $\langle \theta_{mixed}(Y, \tau)\rangle$ for SP forcing at $f = 6$ Hz (head). Note that, since the streamwise vortices form in the braids region, their average mixed fluid temperature should be approximately the average of the two free streams. Indeed, if the streamwise vortices 'entrain' fluid like the spanwise vortices, there is no reason for them to prefer one free stream to the other. Figure 18(*b*) shows a large warm region (corresponding to the head of the streamwise vortex) located on the high-speed side of the cooler primary core.

Figure 19 shows composite images for the SU excitation mode at $f = 3.85$ and 7.7 Hz, including $\langle \text{p.d.f.}(\theta, Y; \tau_i)\rangle$ plots at dimensionless times $\tau = 0.063$, 0.313, 0.563, and 0.813. It is apparent from the data that the mixing process took place in the cores of the pairing primary vortices, with slightly more mixing in the low speed, engulfed

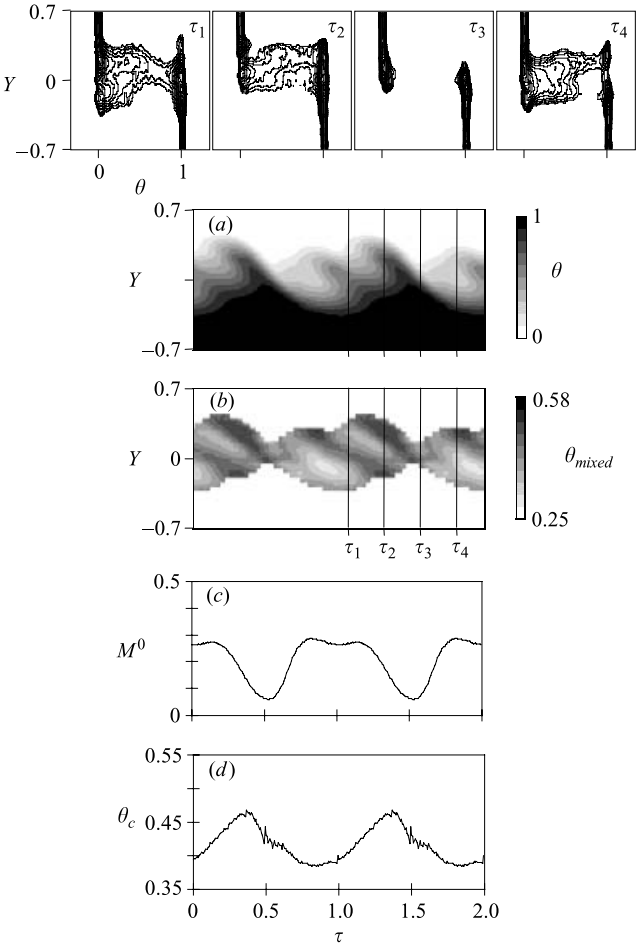

FIGURE 19. Top: $\langle \text{p.d.f.}(\theta, Y; \tau_i) \rangle$ at times $\tau = 0.063$, 0.313, 0.563, and 0.813; (*a*) $\langle \theta(Y, \tau) \rangle$, (*b*) $\langle \theta_{mixed}(Y, \tau) \rangle$, (*c*) $\langle M^0(\tau) \rangle$, and (*d*) $\langle \theta_c(\tau) \rangle$, for SU at $f = 3.85$ and 7.7 Hz. Data are measured at $Rx/\lambda_0 = 3.60$. The contours of $\log_{10}(\langle \text{p.d.f.}(\theta, Y; \tau_i) \rangle)$ begin at a minimum level of −0.523 with a contour increment of 0.1.

vortex, than in the high-speed, engulfing vortex (*c*). Apparently, then, mixed fluid was produced in the low-speed vortex as it was being engulfed by the high-speed vortex, due to the collapse of the laminar layers in the pairing process. Also notice that in the braids region between the sets of pairing spanwise vortices ($\tau = 0.5$), M^0 was actually slightly lower than the minimum of the single-frequency case (0.06 vs. 0.08). This lack of mixed fluid outside the cores of the pairing vortices can also be seen in the almost featureless plot of $\langle \text{p.d.f.}(\theta, Y; \tau_i) \rangle$ at τ_3.

For the case of SP forcing at $f = 3.85$ and 7.7 Hz (head), the streamwise vortex in the braids region between the two pairing rollers was compressed during pairing. In the low-speed (engulfed) vortex (τ_4), there was more mixed fluid than in the high-speed (engulfing) vortex (τ_2). The plot of $\langle M^0(\tau) \rangle$ shows that in the SP case, the local maximum in mixing reached a value of 0.42 in the engulfed vortex and 0.36 in the engulfing vortex. These compare with 0.30 and 0.28, respectively, in the SU case. The fact that the SP forcing increased M^0 more in the engulfed vortex than in the engulfing vortex may seem counterintuitive, as the streamwise vortices between

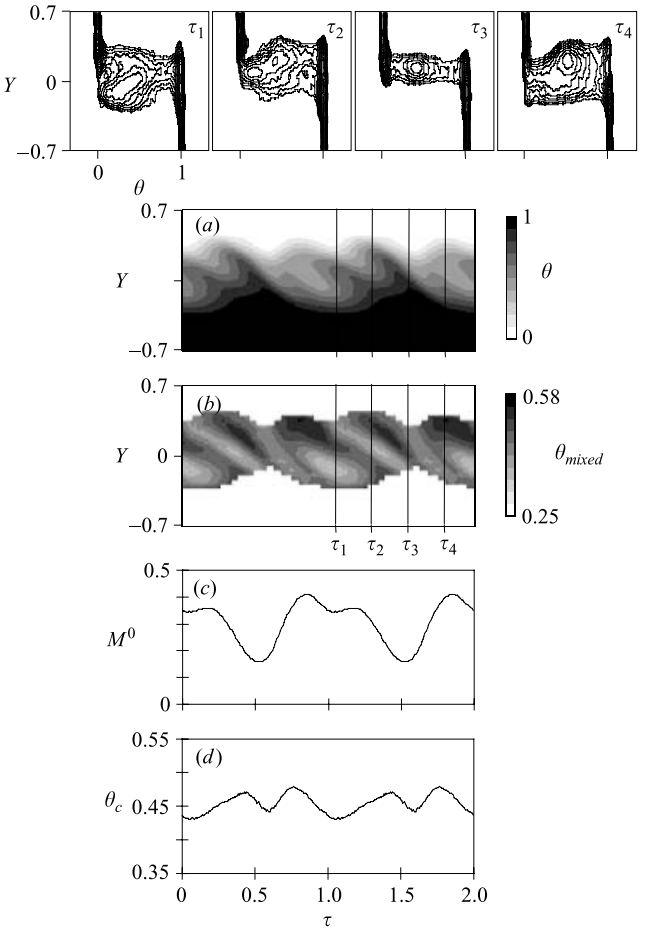

FIGURE 20. Top: $\langle \text{p.d.f.}(\theta, Y; \tau_i)\rangle$ at times $\tau = 0.063$, 0.313, 0.563, and 0.813; (*a*) $\langle\theta(Y, \tau)\rangle$, (*b*) $\langle\theta_{mixed}(Y, \tau)\rangle$, (*c*) $\langle M^0(\tau)\rangle$, and (*d*) $\langle\theta_c(\tau)\rangle$, for SP at $f = 3.85$ and 7.7 Hz (Z_h). Data are measured at $Rx/\lambda_0 = 3.60$. The contours of $\log_{10}(\langle \text{p.d.f.}(\theta, Y; \tau_i)\rangle)$ begin at a minimum level of -0.523 with a contour increment of 0.1.

the pairing primary vortices were being compressed rather than stretched. However, the mixed fluid within the cores of these streamwise vortices was concentrated in regions of diminishing streamwise extent. Thus, at the tail of the streamwise vortex, the largest increase in $\langle M^0(\tau)\rangle$ relative to the SU case occurred at times corresponding to the engulfing vortex (not shown), since the tail of the streamwise vortex was compressed beneath the engulfing vortex.

By comparison, the streamwise vortices in the braids region between the sets of pairing vortices are being stretched. At time τ_3, there is a sharp peak in $\langle \text{p.d.f.}(\theta, Y; \tau_i)\rangle$ at $Y = 0.14$ and $\theta = 0.42$. Mixing occurs over a very narrow cross-stream distance: $-0.04 \leqslant Y \leqslant 0.28$. Recall that the SU pairing case showed a complete lack of mixed fluid between the sets of pairing vortices, suggesting that the mixed fluid in the SP case is due entirely to the effects of the streamwise vortices.

Figure 21 shows $\langle\theta_{mixed}(X, Y; \tau)\rangle$ for SU and SP (at Z_h) excitations at $f = 6$ Hz, and for SU excitation at $f = 3.85$ and 7.7 Hz. The three phase-averaged snapshots in the (X, Y)-plane show the development of the mean mixed temperature with downstream

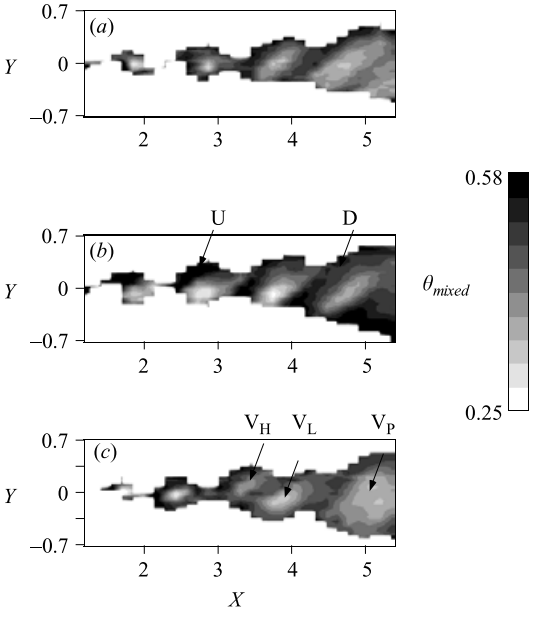

FIGURE 21. $\langle\theta_{mixed}(X, Y; \tau)\rangle$ at $\tau = 0$ for (*a*) SU at $f = 6$ Hz, (*b*) SP at $f = 6$ Hz (Z_h), and (*c*) SU at $f = 3.85$, 7.7 Hz.

distance. In the case of SU forcing at $f = 6$ Hz, there were 'islands' of cool fluid in the centres of the primary vortices that did not diminish with downstream distance. The snapshot of SP forcing at $f = 6$ Hz (figure 21*b*) presents a different scenario: here, at upstream locations (denoted by 'U'), there was a strong temperature gradient between the head of the streamwise vortex and the core of the spanwise vortex. Further downstream (denoted by 'D'), however, streamwise vorticity broke down the primary vortex into smaller scales and mixing activity translated towards the core of the vortex. Concomitantly, the mixed fluid temperature at the core of the roller increased significantly, while the mixed fluid temperature in the streamwise vortex decreased. This trend toward thermal homogeneity is a further manifestation of the increased mixing. Finally, in the case of SU forcing at $f = 3.85$ and 7.7 Hz, the high-speed vortex (denoted by V_H) had a low-temperature island that was slightly warmer than that of the low-speed vortex (denoted by V_L). As these vortices paired, their mixed fluid temperatures equilibrated until, eventually, there remained one large paired vortex (denoted by V_P) whose mixed fluid temperature was approximately the mean of V_L and V_H.

Figure 22 shows $\theta_{mixed}(Y)$ for the unforced flow, SU at $f = 6$ Hz, and SP at $f = 6$ Hz (at Z_h) at three streamwise locations: (*a*) $X = 2.40$, (*b*) 3.60, and (*c*) 4.80. The average temperature profile, $\theta(Y)$, is included for comparison. For the unforced flow, shown on the left, the profiles of θ_{mixed} show a slight variation with cross-stream position. They also depict a minimum near the centre of the layer with slightly higher values toward the outside edges. The finding that $\theta_{mixed}(Y)$ varied only slightly agrees with the results of Konrad (1976) in a gas layer and Koochesfahani & Dimotakis (1986) in a liquid layer, but differs from those of Batt (1977) in a gas layer. Interestingly, the profiles of $\theta_{mixed}(Y)$ for SU forcing, centre, are virtually the same as those for the unforced flow at all three streamwise stations.

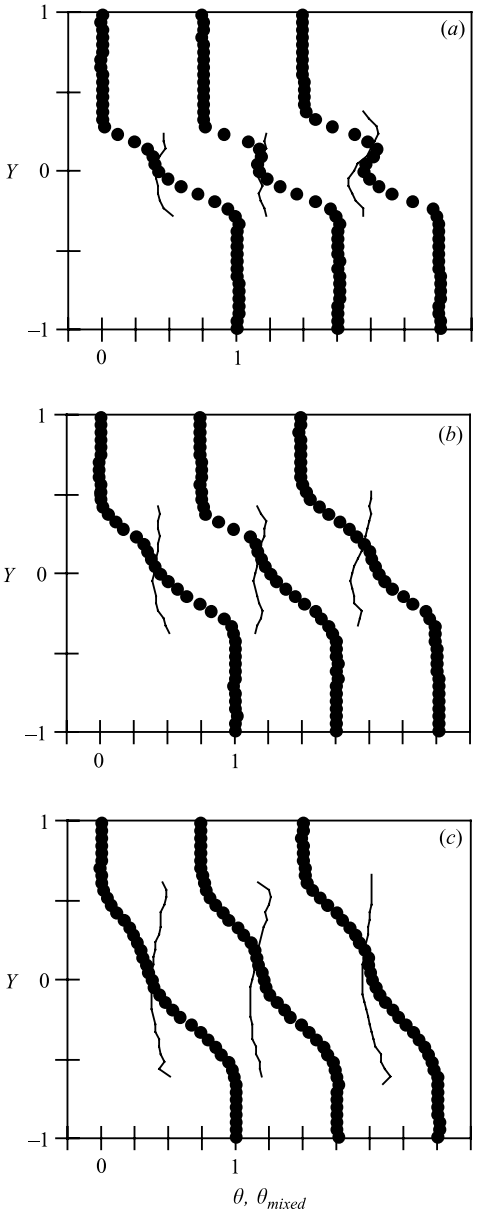

FIGURE 22. Pairs of $\theta_{mixed}(Y)$ (—) and $\theta(Y)$ (●) for unforced (left); SU at $f = 6$ Hz (centre) and SP at $f = 6$ Hz (Z_h) (right) at (*a*) $Rx/\lambda_0 = 2.40$, (*b*) 3.60, and (*c*) 4.80.

The right profiles show θ_{mixed} for SP forcing. The profile at $X = 2.40$ (figure 22*a*) has a zigzag shape with a maximum near the high-speed (low-temperature) side of the layer, and a minimum near the low-speed (high-temperature) side. This may be attributed to the pumping action of the streamwise vortices bringing hot fluid into the layer at the head where it was preferentially mixed. This unique shape of the θ_{mixed} profiles at the head of the streamwise vortices became much less apparent with downstream distance. At $X = 3.60$, the zigzag shape was barely visible, but the entire $\theta_{mixed}(Y)$ profile was tilted in the opposite direction to the mean temperature

profile $\theta(Y)$. Finally, by $X = 4.80$, the $\theta_{mixed}(Y)$ profiles had a similar shape for all three forcing cases, although the SP case had a significantly higher average value of approximately 0.50.

6. Conclusions

In this paper we have shown the effects of forcing (induced pairing and induced spanwise periodicity) on mixing in plane shear layers in the early-to-mid mixing transition region, $1.2 \leqslant Rx/\lambda_0 \leqslant 5.4$. Four primary means of forcing the flow were studied: spanwise uniform (SU) and spanwise periodic (SP) at the fundamental layer frequency ($f = 6$ Hz), and SU and SP with subharmonic pairing ($f = 3.85$ and 7.7 Hz). Scalar concentrations were assessed using a thermal analogue by maintaining a time-invariant temperature difference between the streams upstream of the flow partition. Because of the high diffusivity of temperature in water, the base flow exhibited substantial mixing even in the absence of forcing, consistent with earlier observations of Konrad (1976), Pickett & Ghandhi (2001, 2002), and the 'flame sheet' mixing model of Broadwell & Breidenthal (1982). However, the forcing significantly affected the quantity and the composition of mixed fluid in the layer and accelerated the onset of mixing transition within the domain of measurements.

Spanwise-uniform forcing at the fundamental frequency (6 Hz) inhibited pairing of the primary vortices within a finite streamwise domain, and slightly increased mixed fluid at upstream locations ($Rx/\lambda_0 \leqslant 2.50$). Mixing occurred primarily in the spanwise vortices, starting first at their periphery and then moving towards the centre. The increase in mixing appeared to be due to an earlier rollup of the primary vortices as a result of the forcing, and the effect diminished with downstream distance. Spanwise-periodic forcing at the fundamental frequency (6 Hz) greatly increased mixing (up to 300% at $Rx/\lambda_0 \approx 2.00$) as a result of the formation of spanwise-regular counter-rotating streamwise vortices that were continuously stretched within the braids region between successive primary vortices. Most of the mixed fluid was produced within the induced streamwise vortices, and thus the greatest amount of mixed fluid was measured at a spanwise position midway between the head and the tail of a streamwise vortex where an oblique slice through the streamwise vortex was measured.

The effect of controlled pairing of the primary vortices was investigated by simultaneously forcing at a fundamental frequency and its first harmonic ($f = 3.85$ and 7.7 Hz). Pairing, even with the spanwise-uniform waveform, also increased mixing (by up to 75% at $Rx/\lambda_0 \approx 2.00$). This increase in the amount of mixed fluid was not due to an increase in shear layer width, but rather to improved small-scale mixing, particularly within the core of the engulfed (low-speed) vortex. The merging of the pairing vortices was accompanied by the localized breakdown of their cores. Finally, although spanwise-periodic forcing at $f = 3.85$ and 7.7 Hz increased mixing relative to the spanwise-uniform case, the increase was not as great as in the non-pairing case. Since spanwise periodic forcing at 6 Hz produced more mixed fluid than spanwise periodic forcing at $f = 3.85$ and 7.7 Hz, the effects of pairing and streamwise vorticity interacted unfavourably. This interaction was found to be caused by pairing suppressing (and weakening) the forced streamwise vortices.

It is remarkable that, in all cases except spanwise-uniform forcing at the fundamental frequency, the increase in mixing due to the forcing showed no sign of diminishing at the end of the test section, $X = 5.40$. This suggests that provided the forcing waveform is properly amplified, it can lead to enhanced mixing throughout most of the mixing transition region.

Through the use of phase-locked measurements, we were also able to draw conclusions about the composition of mixed fluid within the layer under the various forcing waveforms. These measurements showed that around the periphery of the primary vortices fluid mixed at nearly the average concentration of the two free streams. However, within the cores of the spanwise vortices, fluid mixed at a concentration nearer to that of the high-speed stream due to the preferential entrainment of high-speed vs. low-speed fluid into the layer. Because mixing began at the periphery of the spanwise vortices in the case of spanwise-uniform forcing at $f = 6\,\mathrm{Hz}$, and then migrated to the centre of the vortex with increasing downstream distance, the average mixed fluid concentration moved toward the high-speed concentration with increasing downstream distance. The same trend appeared in the unforced flow as well. However, in the braids region between the spanwise vortices, fluid mixed at a concentration near the average of the two free streams. This was expected, since there was no asymmetry with respect to the free streams. For this reason, spanwise-periodic forcing led to mixed fluid near the average concentration of the two free streams. Thus, in contrast to spanwise-uniform forcing, spanwise-periodic forcing caused the mixed fluid concentration to move towards that of the low-speed stream with increasing downstream distance. The concentration approached a value of $\theta_c = 0.5$ at $Rx/\lambda_0 = 5.40$, but did not reach an asymptote by the end of the test section.

This work was supported by AFOSR. The authors would like to acknowledge a number of useful discussions with Professor Arne Pearlstein.

REFERENCES

Batt, R. G. 1977 Turbulent mixing of passive and chemically reacting species in a low-speed shear layer. *J. Fluid Mech.* **82**, 53–95.

Bernal, L. P. & Roshko, A. 1986 Streamwise vortex structure in plane mixing layers, *J. Fluid Mech.* **170**, 499–525.

Breidenthal, R. 1981 Structure in turbulent mixing layers and wakes using a chemical reaction. *J. Fluid Mech.* **109**, 1–24.

Broadwell, J. E. & Breidenthal, R. E. 1982 A simple model of mixing and chemical reaction in a turbulent shear layer. *J. Fluid Mech.* **125**, 397–410.

Buell, J. C. & Mansour, N. N. 1989 Asymmetric effects in three-dimensional spatially-developing mixing layers. *Seventh Symp. on Turbulent Shear Flows, Stanford University, August 21–23, 1989*, pp. 9.2.1–9.2.6.

Dimotakis, P. E. 1986 Two-dimensional shear-layer entrainment. *AIAA J.* **24**, 1791–1796.

Dimotakis, P. E. 1989 Turbulent free shear layer mixing. *AIAA Paper* 89-0262.

Dimotakis, P. E. 2000 The mixing transition in turbulent flows. *J. Fluid Mech.* **409**, 69–98.

Huang, L.-S. & Ho, C.-M. 1990 Small-scale transition in a plane mixing layer. *J. Fluid Mech.* **210**, 475–500.

Karasso, P. S. & Mungal, M. G. 1996 Scalar mixing and reaction in plane liquid shear layers. *J. Fluid Mech.* **323**, 23.

Katch, G. J. & Koochesfahani, M. M. 1993 Mixing of species in a two-stream shear layer forced by an oscillating airfoil. *AIAA Paper* 93-0444.

Konrad, J. H. 1976 An experimental investigation of mixing in two-dimensional turbulent shear flows with applications to diffusion-limited chemical reactions. PhD thesis, California Institute of Technology.

Koochesfahani, M. M. & Dimotakis, P. E. 1986 Mixing and chemical reactions in a turbulent liquid mixing layer. *J. Fluid Mech.* **170**, 83–112.

Koochesfahani, M. M. & MacKinnon, C. G. 1991 Influence of forcing on the composition of mixed fluid in a two-stream shear layer. *Phys. Fluids* A **3**, 1135–1142.

Liepmann, H. W., Brown, G. L. & Nosenchuck, D. M. 1982 Control of laminar instability waves using a new technique. *J. Fluid Mech.* **118**, 187–200.

Masutani, S. M. & Bowman, C. T. 1986 The structure of a chemically reacting plane mixing layer. *J. Fluid Mech.* **172**, 93–126.

Moser, R. D. & Rodgers, M. M. 1993 The three-dimensional evolution of a plane mixing layer: pairing and transition to turbulence. *J. Fluid Mech.* **247**, 275–320.

Mungal, M. G. & Dimotakis, P. E. 1984 Mixing and combustion with low heat release in a turbulent shear layer. *J. Fluid Mech.* **148**, 349–382.

Nygaard, K. J. & Glezer, A. 1991 Evolution of streamwise vortices and generation of small-scale motion in a plane shear layer. *J. Fluid Mech.* **231**, 257–301.

Oster, D. & Wygnanski, I. 1982 The forced mixing layer between parallel streams. *J. Fluid Mech.* **123**, 91–130.

Park, K.-H., Metcalfe, R. W. & Hussain, F. 1994 Role of coherent structures in and isothermally reacting mixing layer. *Phys. Fluids* A **6**, 885–902.

Perry, A. E. 1982 *Hot-wire Anemometry*. Oxford University Press.

Pickett, L. M. & Ghandhi, J. B. 2001 Passive scalar measurements in a planar mixing layer by PLIF of acetone. *Exps. Fluids* **31**, 309–318.

Pickett, L. M. & Ghandhi, J. B. 2002 Passive scalar mixing in a planar shear layer with laminar and turbulent inlet conditions. *Phys. Fluids* **14**, 985–998.

Roberts, F. A. & Roshko, A. 1985 Effects of periodic forcing on mixing in turbulent shear layers and wakes. *AIAA Shear Flow Control Conference, March 12–14, Boulder, Colorado.*

Wiltse, J. M. 1993 Control of mixing in a nonreactive plane shear layer. PhD thesis, University of Arizona.

Winant, C. D. & Browand, F. K. 1974 Vortex pairing: the mechanism of turbulent mixing-layer growth at moderate Reynolds number. *J. Fluid Mech.* **63**, 237–255.